

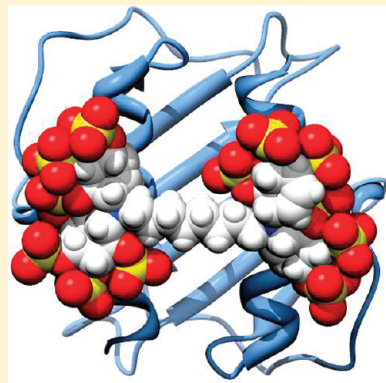
Molecular Dynamics Simulations of CXCL-8 and Its Interactions with a Receptor Peptide, Heparin Fragments, and Sulfated Linked Cyclitols

Neha S. Gandhi^{†,‡} and Ricardo L. Mancera^{*,†,‡,§}

[†]Curtin Health Innovation Research Institute, Western Australian Biomedical Research Institute, [‡]School of Biomedical Sciences, and [§]School of Pharmacy, Curtin University, GPO Box U1987, Perth WA 6845, Australia.

 Supporting Information

ABSTRACT: CXCL-8 (Interleukin 8) is a CXC chemokine with a central role in the human immune response. We have undertaken extensive in silico analyses to elucidate the interactions of CXCL-8 with its various binding partners, which are crucial for its biological function. Sequence and structure analyses showed that residues in the third β -sheet and basic residues in the heparin binding site are highly variable, while residues in the second β -sheet are highly conserved. Molecular dynamics simulations in aqueous solution of dimeric CXCL-8 have been performed with starting geometries from both X-ray and NMR structures. Simulations showed shearing movements between the two antiparallel C-terminal helices. Dynamic conservation analyses of these simulations agreed with experimental data indicating that structural differences between the two structures at quaternary level arise from changes in the secondary structure of the N-terminal loop, the 3_{10} -helix, the 30s, 40s, and 50s loops and the third β -sheet, resulting in a different interhelical separation. Nevertheless, the observation of these different states indicates that CXCL-8 has the potential to undergo conformational changes, and it seems likely that this feature is relevant to the mode of binding of glycosaminoglycan (GAG) mimetics such as cyclitols. Simulations of the receptor peptide fragment–CXCL-8 complex identified several specific interactions of the receptor peptide with CXCL-8 that could be exploited in the structure-based design of competitive peptides and nonpeptidic molecules targeting CXCL-8 for combating inflammatory diseases. Simulations of the CXCL-8 dimer complexed with a 24-mer heparin fragment and of the CXCL-8–receptor peptide complex revealed that Arg60, Lys64, and Arg68 in the dimer bind to cyclitols in a horseshoe pattern, defining a region which is spatially distinct from the receptor binding site. There appears to be an optimum number of sulfates and an optimum length of alkyl spacers required for the interaction of cyclitol inhibitors with the dimeric form of CXCL-8. Calculation of the binding affinities of cyclitol inhibitors reflected satisfactorily the ranking of experimentally determined inhibitory potencies. The findings of these molecular modeling studies will help in the search for inhibitors which can modulate various CXCL-8 biological activities and serve as an excellent model system to study CXC-inhibitor interactions.



INTRODUCTION

CXCL-8 (Interleukin-8/IL-8) is a pro-inflammatory chemokine produced by various types of cells upon inflammatory stimuli.¹ It is secreted by endothelial and epithelial cells, fibroblasts, neutrophils, T lymphocytes, hepatocytes, keratinocytes, and peripheral blood monocytes.² CXCL-8 has a major role in neutrophil recruitment to and activation at the inflammation site where it enhances the adherence of circulating neutrophils to endothelial cells involving proteoglycans and subendothelial matrix proteins.³ A series of cell-physiological responses required for neutrophil migration and its target function phagocytosis are also induced, like calcium mobilization, actin polymerization, degranulation, and respiratory burst.^{2,4–6} CXCL-8 can then establish a concentration gradient to direct leukocytes to migrate across the endothelium and through the extracellular matrix into the tissue.⁷ Because neutrophils are principal effector cells in acute ischemia-reperfusion injury, CXCL-8 has gained a major focus in transplantation research.^{8,9} CXCL-8 has also been reported as a pro-inflammatory mediator in dermatologic diseases such as psoriasis.¹⁰ In the context of inflammatory diseases of the lung, the concentration of CXCL-8 in bronchoalveolar

lavage fluid from patients with idiopathic pulmonary fibrosis, bacterial pneumonia, and the acute respiratory distress syndrome is usually elevated and is associated with increased mortality.^{11–14} CXCL-8 is thus an important mediator in the innate immune system response by acting as a potent chemo-attractant for neutrophils.¹ CXCL-8 is also known to promote angiogenesis and tumor metastasis.^{15,16}

Interleukin-8 (IL-8) is the older name for CXCL-8, which received its name¹⁷ based on the so-called CXC-chemokines (wherein the two N-terminal cysteines of chemokines are separated by one amino acid, represented in this name with an “X”).¹⁸ The CXCL-8 protein is encoded by the SCYB8 (small inducible cytokine subfamily B member 8) gene. CXCL-8 is generated as a precursor of 99 amino acids and is secreted after cleavage of a signal sequence of 20 residues. Several N-terminal processed forms are produced by proteolytic cleavage after secretion from peripheral blood monocytes, leukocytes, and endothelial cells, but possibly other cells too.

Received: August 30, 2010

Published: February 07, 2011

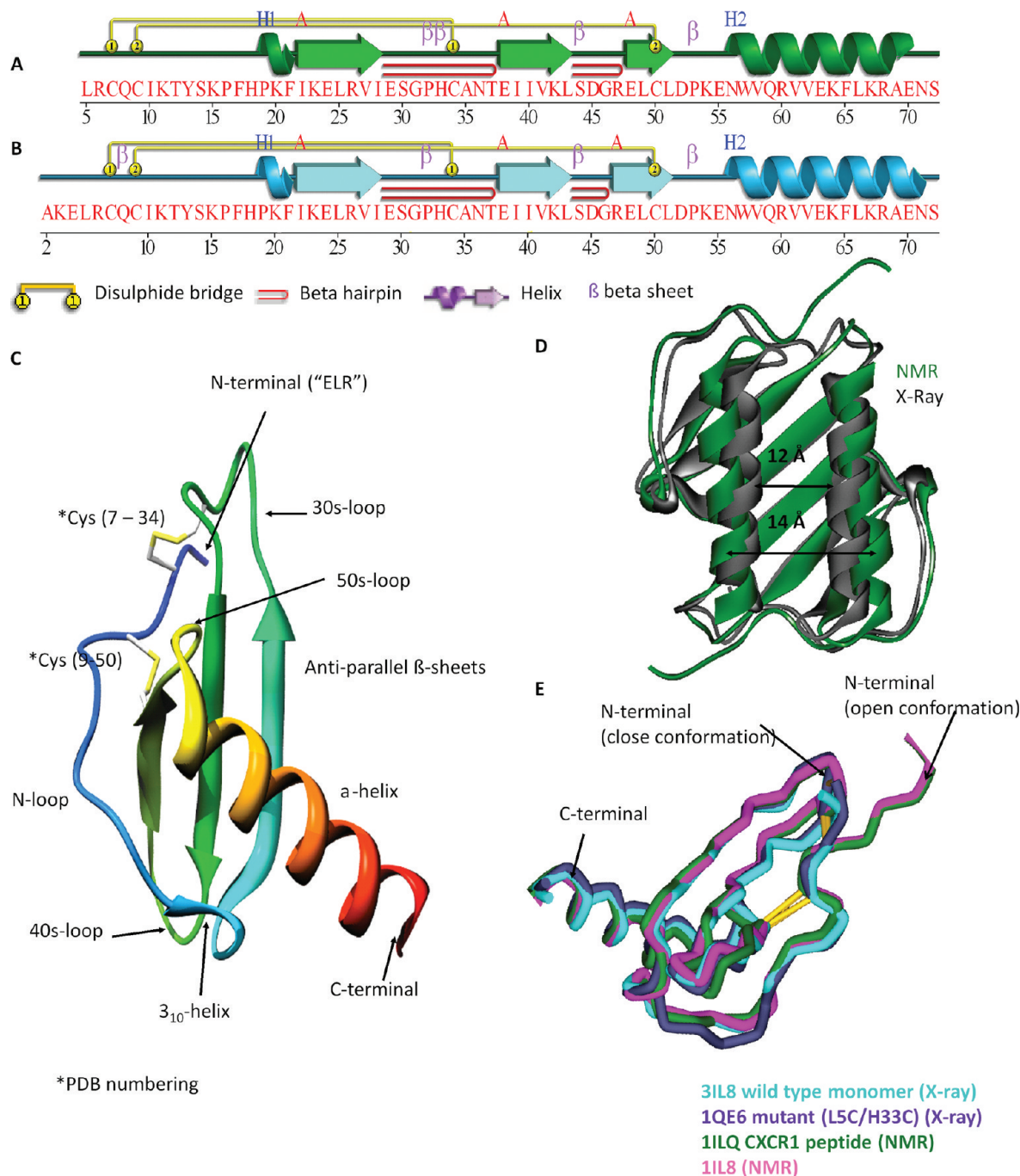


Figure 1. (A) Secondary structure representation of the structure of CXCL-8 (PDB code: 3IL8). (B) Secondary structure representation of the structure of CXCL-8 (PDB code: 1IL8). H1 indicates a 3_{10} -helix located before the first β -strand, and H2 indicates the C-terminal helix, while the symbol " β " represents the presence of β -sheets in both parts A and B. The disulfide connectivity in the N-loop is represented by yellow lines. (C) Ribbon diagram of the CXCL-8 structure. (D) C-terminal helices: closer in the X-ray structure compared to the NMR structure. (E) Superimposition of the backbone of the various NMR and X-ray structures of CXCL-8 revealing differences in the conformation of the N-loop.

CXCL-8 possess conserved amino acids that are important for its tertiary structure, such as the Greek Key motif shown in Figure 1, a single-turn helix (3_{10} -helix), three antiparallel β -strands, and a C-terminal α -helix. The Greek Key motif, which features four β -sheets, is characteristic of chemokines, but there are only three β -sheets in monomeric CXCL-8.¹⁹ CXCL-8 has two conserved disulfide bridges between Cys7 and Cys34 and between Cys9 and Cys50 (PDB numbering). These four conserved cysteines stabilize the structure of CXCL-8.^{20,21} Cys7 and

Cys9 are situated close together near the N-terminus of the mature protein, while Cys34 resides at the center of the protein and Cys50 is located before the C-terminal helix. A loop of approximately 10 amino acids is located after Cys7 and Cys9, known as the N-loop. These helices and strands are connected by turns called 30s, 40s, and 50s loops. Cys61 and Cys77 are located, respectively, in the 30s and 50s loops.¹⁹ The C-terminal α -helix plays a functional role in heparin binding and receptor interaction.²²⁻²⁴

The structural analysis of CXCL-8 by NMR spectroscopy^{25–27} and X-ray diffraction^{28,29} has revealed that CXCL-8 exists as a homodimer at high concentrations. Mutant and chimeric structures of CXCL-8 have also been reported.^{30,31} The CXCL-8 dimer consists of two α -helices oriented in an antiparallel fashion on top of six β -sheets with the interactions at the dimerization interface consisting of main-chain hydrogen bonding (amino acids from position 23 to 29) between a β -sheet in each monomer. The structure of the monomer is similar to that of the monomeric subunit in the dimer, except that the C-terminal helical residues that are structured in the dimer are unstructured in the monomer.²⁷ There have been conflicting reports about the inter-relationship between CXCL-8 monomer–dimer equilibrium and their differential binding affinities for CXCR1, CXCR2, and glycosaminoglycans (GAGs), which appear to depend on the *in vivo* and *in vitro* conditions.^{32–35} It has been reported that the dimerization constant for wild type CXCL-8 has a value of about 10–20 μM under physiological ionic strength, pH, and temperature conditions,^{36,37} with this value being highly sensitive to specific solution conditions.³⁸ A dimerization constant of 120 nM has also been reported.³⁹ In addition to CXCL-8 homodimerization, CXCL-8 can also form heterodimers with other chemokines, such as platelet factor 4 (PF4) or CXCL-4.⁴⁰

Few but important differences have been observed between the X-ray and NMR structures of CXCL-8. The secondary structure representations of the sequence of CXCL-8 in both the X-ray (PDB code: 3IL8) and NMR (PDB code: 1IL8) structures are shown in Figure 1. The principal difference between the NMR and X-ray structures of the CXCL-8 dimer is the distance between the α -helices (Figure 1D). The center-to-center distance between the antiparallel helices is about 12 Å in the X-ray structure and about 14 Å in the NMR structure.²⁸ Previous molecular dynamics (MD) simulations in implicit solvent have suggested that the helices in the NMR structure can move closer together, resulting in an interhelical distance that more closely resembles that observed in the X-ray structure.⁴¹ Knowing which interhelical distance is more realistic is crucial for predicting and understanding the binding of ligands to CXCL-8.

Another difference between the X-ray and NMR structures is the presence of different conformations of the N-loop and N-terminal up to the first cysteine.^{26,28} Two distinct conformations (Figure 1E) can be defined: closed (with the N-loop in close proximity to the α -helix) and open (with the N-loop further away from the α -helix and near Arg47).^{25,28,30,31} In the closed conformation, a hydrophobic pocket between the N-loop and Arg47 is exposed, whereas a proline residue occupies this region in the open conformation.²³

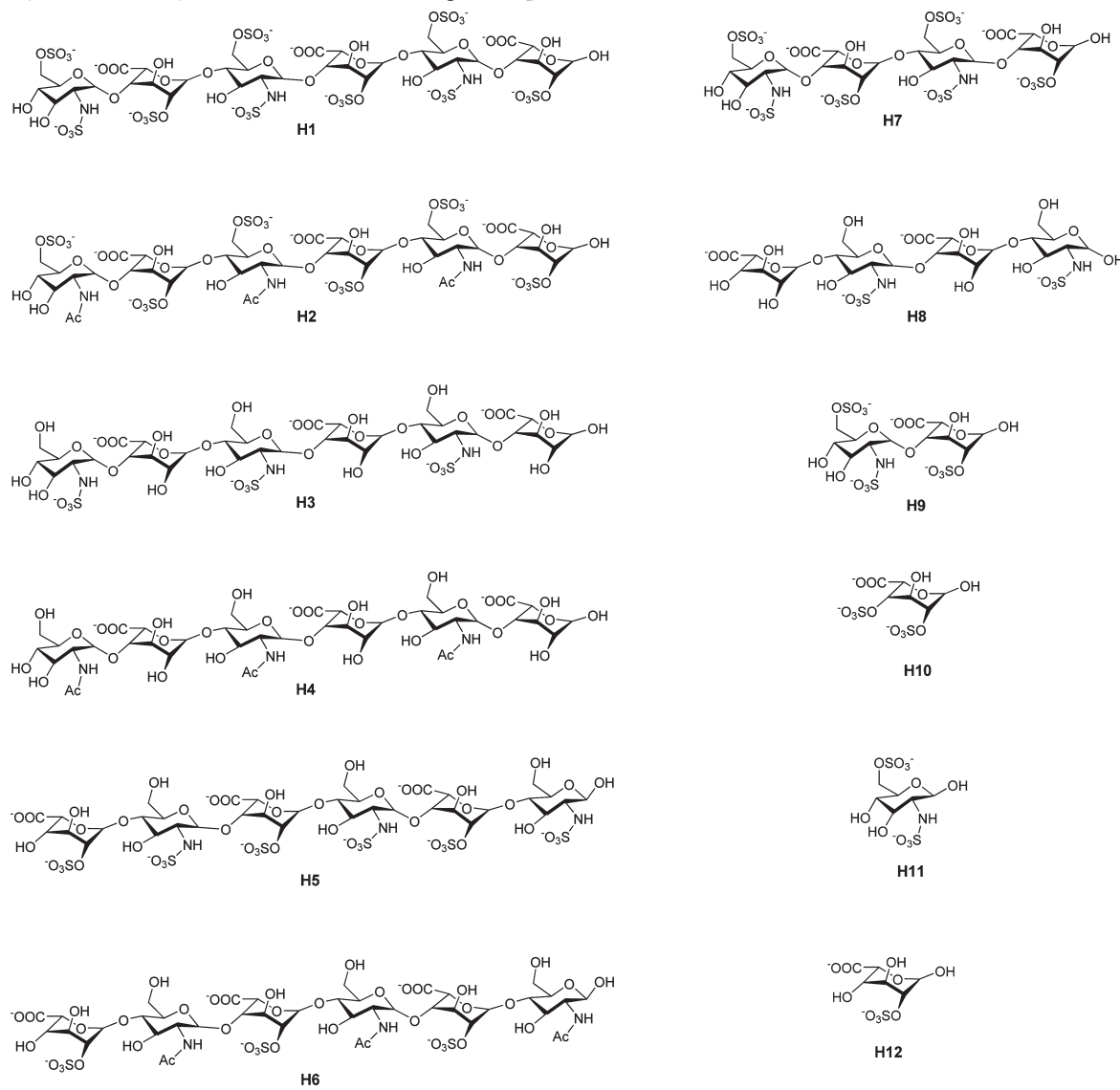
Another important difference between the NMR and X-ray structures is the position and protonation of histidine residues. In the NMR (solution) structures, both His18 and His33 have low pK_a values [3.7 and 4.9, respectively].²⁶ In the X-ray structure, the Nε2 atom of His33 donates a hydrogen bond to the carbonyl in the backbone of Glu29, whereas in the low resolution NMR structure the side-chain of His33 is incorrectly placed and Arg6 has incorrect (nonplanar) χ -5 dihedral angle values. Hence, we focused our analysis on the more reliable X-ray structure of CXCL-8. In both structures, His18 makes the same hydrogen bond with the amide nitrogen of Lys20.

CXCL-8 carries out its regulatory role by binding and activating two homologous G-protein coupled receptors (GPCRs),^{42–44} namely CXCR1 (IL-8 receptor A or IL-8 receptor type 1 or IL-8R α) and CXCR2 (IL-8 receptor B or IL-8 receptor type 2 or IL-8R β) in humans, with affinities of 3.6 nM.⁴⁵ Mice express only the CXCR2 receptor on neutrophils. The CXCL-8 monomer and

dimer differentially activate and regulate CXCR1 and CXCR2 receptors. CXCR1 binds with high affinity only to CXCL-8 while CXCR2 binds to multiple chemokines, such as the epithelial cell-derived neutrophil activator (ENA-78), neutrophil activating peptide-2, and the GRO subfamily of proteins (GRO- α , GRO- β , and GRO- γ).⁴⁶ CXCL-8 also binds to the promiscuous Duffy antigen/receptor for chemokines (DARC) found on the surface of erythrocytes, with an affinity of approximately 20 nM.⁴⁷ Mutagenesis experiments have identified the specific interactions between the N-loop of CXCL-8, including the triad Glu-Leu-Arg ("ELR"), and the N-terminal domains (site I or primary site),⁴⁸ and the III and IV extracellular loops (site II or secondary site)²³ of the chemokine receptors, which determine the receptor trafficking profiles. Selectivity and signaling specificity is achieved by the N-terminal domains of the receptors and their ligands.^{49–51} The NMR structure of wild type CXCL-8 dimer (and not the functionally relevant monomer) complexed with a peptide analogue of CXCR1 (a receptor peptide) has been published.²⁵ This receptor fragment shows relatively potent inhibition of CXCL-8 receptor binding ($K_i = 7 \mu\text{M}$).⁵² The NMR structure revealed the interaction to be primarily hydrophobic and mediated by side-chains involving amino acids Gln8, Ile10, Lys11, Tyr13, Phe17, Phe21, Ile40, Leu43, Arg47, and Leu49 present in the N-terminal region of CXCL-8,²⁵ whereas the side-chains of Asp5 and the amine capping residue NH₂ of the receptor peptide make hydrogen bonds with Lys20 and Gln8 of CXCL-8, respectively. Mutational studies of CXCR1 have identified Arg199 and Arg203 on the third extracellular loop and Asp265 on the fourth extracellular loop as being important for CXCL-8 binding,⁵³ whereas the receptor binding site on the surface of CXCL-8 comprises residues on the third β -sheet (Glu48 to Cys50), the turn preceding the third β -sheet (Ser44), one residue on the C-terminal α -helix (Val61) and residues starting from Lys15 in the N-terminal region.⁵⁴ The interactions of CXCR1 domain with the CXCL-8 monomer were distinctly different from the dimer.^{54,55} On the basis of the binding of a monomeric CXCL-8 to CXCR1 N-domain, only N-loop residues of CXCL-8 were found to be involved in direct binding whereas residues in any other region (such as Val61 and Ser44) is due to indirect coupling interactions in the dimer. Molecular modeling studies of the interaction of CXCL-8 with CXCR2⁵⁶ have suggested that the N-terminus of CXCR2 binds to the N-terminus of CXCL-8 (site I or primary site), while extracellular loops III and IV of CXCR2 bind to the C-terminal helix of CXCL-8 (site II or secondary site).

CXCL-8 is known to bind heparin/heparan sulfate (HS) present on the endothelial cell surface and basement membrane.²² Heparin/HS play an important role in the promotion of CXCL-8 dependent transmigration of neutrophils and the protection of the tissue microenvironment from cleavage by enzymes, such as elastase released from migrating cells. The addition of HS or heparin to CXCL-8 has also been shown to prevent CXCL-8 from unfolding, thereby suggesting a role for glycosaminoglycans (GAGs) on CXCL-8 stability and protection from proteolytic degradation *in vivo*.³⁹ Amino acids involved in heparin binding include Arg60, Lys64, Lys67, and Arg68, which are located within the C-terminal α -helix, as well as His18 and Lys20, which are located in the proximal loop.⁵⁷ Dimeric CXCL-8 requires 5–6 trisulfated saccharides (sulfated domain) to bind to each monomer,⁵⁸ connected by a flexible linker consisting of 12–14 sugar residues (N-acetylated) [Figure S1 of the Supporting Information]. This heparin fragment is believed to adopt a horseshoe arrangement wherein each sulfated domain interacts with the antiparallel CXCL-8 dimer.⁵⁹ It has been reported that homodimerization of CXCL-8 is required for heparin binding, whereas monomeric CXCL-8 is capable of binding to its

Table 1. Synthetic Library of Amine-Terminated Sugar—Heparin Derivatives



receptors without loss of affinity.^{60–63} Earlier molecular modeling studies on the binding of heparin to monomeric and dimeric CXCL-8 correlated well with experimental data, identifying the putative amino acids and the length of GAG fragments required for interaction with CXCL-8.^{64–66} The ranking of these residues in terms of their contributions to GAG binding was determined to be Lys64, Arg60, Lys20, Lys67, Arg68, and His18.⁶⁴

The GAG-binding region is essentially distinct from the receptor-binding region, suggesting that CXCL-8 may bind to its receptor in the presence of GAGs.⁵⁷ Conflicting reports have emerged regarding the length of heparin fragments required for binding to CXCL-8.^{39,58,64} The dissociation constant (K_d) of heparin fragments to CXCL-8 has been investigated using isothermal titration calorimetry and determined to be 0.39–2.63 μM , with five saccharide units required to bind to each monomer.⁵⁸ In the same study, the binding affinity of heparin to CXCL-8 was shown to increase with increasing chain length. In addition, O-sulfation in heparin fragments was found to be more important than N-sulfation for binding to CXCL-8. Nonetheless, another study found the existence of a periodic pattern for the

dissociation constants of heparin oligosaccharides with respect to chain length.³⁹ GAG disaccharides were identified to be the minimum length required for binding to CXCL-8. Isothermal fluorescence titration was used to estimate the binding affinities of heparin/HS oligosaccharides of various lengths, and these were found to be dependent on the oligomerization state of CXCL-8. High affinity binding of heparin/HS was reported for monomeric CXCL-8 while low affinity was reported for the dimeric form.

Soluble heparin/HS are known to inhibit binding of CXCL-8 to its receptors, blocking its biological activity. By contrast, cell surface heparin/HS help present chemokines to their GPCRs by increasing the local concentration of protein.⁵⁸ Heparin-based molecules from a synthetic library of amine-terminated sugars have also been reported to block the formation of chemokine gradients on the cell surface.⁶⁷ We henceforth refer to these oligosaccharides as H1 to H12 [Table 1]. Experiments showed that CXCL-8 binds oligosaccharides H1, H2, H5, H6, H7, H9, and H10. In addition, the binding of hexasaccharide H6 suggested that the 2-O-sulfate groups in alpha-L-iduronate (IdoA)

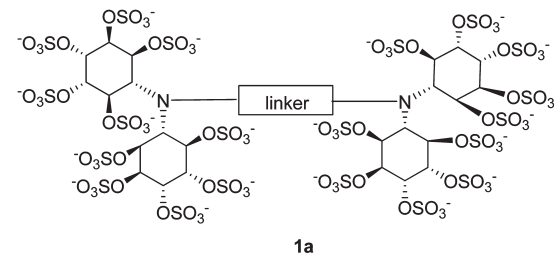
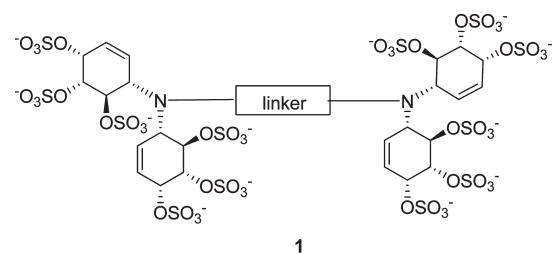
units play an important role in this interaction. The binding affinity of synthetic oligosaccharides as short as disaccharide H9 was attributed to multivalent and cooperative interactions present on the chemokine surface, as opposed to the horseshoe arrangement proposed earlier.⁵⁹

Several approaches have been pursued in the last two decades in order to identify molecules which can modulate the biological activities of CXCL-8.^{9,68} Peptide-mimetics based on the CXCL-8 scaffold have been reported to block the actions of CXCL-8. In view of the critical role of the N-terminal domain, antagonists of CXCL-8 have been developed either by truncating the amino-terminal of CXCL-8 or by modifying the amino acids in the ELR+ motif at the N-terminus. These modified CXCL-8 derivatives bind both CXCR1 and CXCR2 and inhibit CXCL-8 mediated neutrophil responses.^{69–71} Alternatively, mimicking the receptor rather than the ligand has also been reported.⁷² The identification and role of small molecules capable of selectively blocking CXCL-8 receptors has also been reviewed.^{9,68,73} Compared to low molecular weight chemokine receptor antagonists, which generally target leukocytes, another novel approach is to design molecules to interfere with wild-type chemokine signaling at the endothelium by masking endothelial GAGs with non-GPCR-binding CXCL-8. Recently, a dnCXCL-8 (dominant negative CXCL-8) functional antagonist was shown to exhibit significantly increased binding affinity for GAG structures on endothelial surfaces, which can significantly compete with wild-type CXCL-8 from endothelial GAGs.^{74,75} In addition, the natural GPCR binding motif to CXCR1/2 was knocked out in dnCXCL8, resulting in a decoy protein.

Carbohydrate mimetics that bind to CXCL-8 and inhibit its biological activity have been reported.⁷⁶ These molecules are alkyl-linked tetrameric cyclitols [Table 2] that require at least a 7-carbon long spacer in order to bind to CXCL-8. Cyclitols are pseudosugars in which the pyranosyl-ring oxygen has been replaced by a methylene unit. Such compounds are highly stable and do not suffer from glycosidic cleavage. Four of the 15 reported sulfated cyclitols, i.e. numbers 8, 9, 10, and 10a, blocked effectively the CXCL-8-heparin interaction, with the remaining 11 compounds showing no activity. Cyclitol 8 displayed an IC₅₀ of 50 nM, and cyclitols 9 and 10 were also quite strong inhibitors, although not as effective as compound 8. The highly sulfated cyclitol 10a showed comparable inhibition to 10.

In this paper, we report a series of structural bioinformatics and molecular modeling studies aimed at characterizing the interactions of CXCL-8 with its various binding partners. We have analyzed the evolutionary conservation of amino acid positions in human CXCL-8 by comparing 39 protein sequences to identify structurally and functionally important regions for interactions with its receptors and GAGs. We have also carried out molecular dynamics (MD) simulations in aqueous solution of the dimer of CXCL-8 with starting geometries from both its X-ray and NMR structures and monitor the changes in the secondary structure of the CXCL-8 dimer. These analyses were further extended to identify the region which contributes mostly to the conformational flexibility of the CXCL-8 dimer. MD simulations based on structural data of a complex of CXCL-8 to a receptor peptide fragment identified extended interaction sites within the protein–protein interface upon conformational changes. We have also performed molecular docking simulations of various heparin oligosaccharides to the CXCL-8 monomer and dimer. Since no structural determinations have been

Table 2. Structures of the Various Sulfated Linked Cyclitols



Molecule	Linker
2-10	-(CH ₂) _n - where n = 2-10
6a	-(CH ₂) ₆ -
10a	-(CH ₂) ₁₀ -
11	
12	
13	
14	

reported for bound complexes of cyclitols with CXCL-8, we have also modeled their interactions with CXCL-8 oligomers.

MATERIALS AND METHODS

Sequence and Structural Analyses. A PSI-BLAST⁷⁷ search was performed against the SWISS-PROT database.⁷⁸ The query sequence corresponds to the CXCL-8 human sequence (P10145). The resulting sequences, species, SWISS-PROT⁷⁸ accession numbers, and sequence identity with reference to human CXCL-8 are listed in Supporting Information Table S1.

A ConSurf⁷⁹ analysis of the evolutionary conservation profile of CXCL-8 (PDB code 3IL8) was carried out to identify putative functional regions. The phylogenetic tree produced by Consurf was plotted using FigTree 1.2.2.⁸⁰ More details about this method are provided in the Supporting Information.

Normal Modes Analysis (NMA). NMA was used to predict the low frequency, high amplitude interdomain equilibrium motions of the CXCL-8 dimer using the Elastic Network Model (ENM), as available through the ElNémo web server.⁸¹ PDB

structures 3IL8 and 1IL8 were used as input for these calculations. The lowest frequency normal modes were computed with the minimum and maximum perturbations set to -150 and 150 DQ, respectively, to amplify molecular motions.

Electrostatic Potential Surface. Electrostatic potential calculations were done using the DELPHI program implemented in DS Modeling 2.1 (Accelrys, Inc.) using the atomic partial charges assigned by CFF,⁸² with a protein interior dielectric constant of 1, a solvent dielectric constant of 80, and an ionic strength of 0.145 M.

Sulfate Binding Motif Search. The presence of sulfate ions (originating from the crystallization buffer) on the surface of a protein structure determined by X-ray diffraction may suggest the presence of GAG binding sites, as is the case with mutant CXCL-8,³⁰ SDF-1 α ,⁸³ MCP-1,⁸⁴ and RANTES.⁸⁵ Sequence analysis combined with fold recognition methods can also help to predict sulfate binding motifs in GAG-binding proteins.⁸⁶ A search for structural homologues of CXCL-8 was performed using the SSM server^{87,88} to look for structures with similar folds. PDB structure 1QE6³⁰ was used as a query. Pairwise comparison and 3D alignment of protein structures were carried out considering a structural homology of 25% or more. The results were manually screened for structures which had been crystallized with sulfate ions or sulfated ligands.

Molecular Docking. The chemical structures of heparin H1–H12, 24-mer fragment, and cyclitols were sketched in Chemdraw Ultra 11.0⁸⁹ and saved in MDL molfile format. The program OMEGA v.2.3.2⁹⁰ was used to convert all heparin and cyclitol structures to 3D multiconformer structures and to add hydrogen atoms and partial charges using the MMFF force-field.^{91–95} The maximum number of conformers (maxconfs) was set to 50. OMEGA was used because of its ability to enumerate ring conformations and invertible nitrogen atoms. This method is useful in enumerating ring conformations in heparin, particularly sulfated alpha-L-iduronate (IdoA2S) residues which may adopt skew boat (²S₀) and chair (¹C₄) conformations.⁹⁶

The FRED⁹⁷ molecular docking engine takes a multiconformer database of one or more ligands generated by OMEGA, a target protein structure, a box defining the active site of the protein on the basis of a ligand–protein complex and several optional parameters as input. The binding pocket was defined using the ligand-free CXCL-8 X-ray structure (PDB code: 3IL8) and the NMR structure (PDB code: 1IL8) using FRED-Receptor (Eyes Open, Inc.). The protein was prepared using the MMFF force-field in FRED. Three different binding sites were defined: site 1, parallel to the alpha helices (monomer); site 2, perpendicular to the alpha helices (dimer); and site 3, blind docking wherein the whole CXCL-8 dimer was enclosed in the box. FRED⁹⁷ was used because of its ability to dock large flexible ligands in large binding sites.⁹⁸ The inner contour (a shape complementary to the active site, used during the exhaustive search) was disabled as the binding sites in GAG-binding proteins consist of clefts or sets of juxtaposed surface residues rather than pockets.⁹⁹ The ligand conformers were kept flexible whereas protein structure was treated as rigid during the docking simulations. The number of poses (num_poses) to be returned by the exhaustive search was set to 300, defined as the top scoring poses selected from the list of all poses and scored by the scoring functions specified by the exhaustive scoring. The number of alternative poses (num_alt_poses) was set to 100, defined as additional poses to the top consensus structure poses.

In the optimization step, four scoring functions were used: ChemGauss,⁹⁷ ChemScore,¹⁰⁰ PLP,¹⁰¹ and ScreenScore.¹⁰² Binding poses obtained from FRED using the consensus score were extracted. The Gaussian shape fitting function¹⁰³ was not used. AutoDock has been used successfully to dock and score heparin–protein

complexes,^{66,86} and hence, the consensus binding poses were redocked with AutoDock 4.0¹⁰⁴ using AutoDock's Lamarckian genetic algorithm with a population of 200 individuals and 50×10^6 energy evaluations. The grid box was defined with a constant grid spacing of 0.37 Å around each ligand molecule using the previous obtained consensus binding pose. The AutoDock 4.0 scoring function¹⁰⁵ was used to predict inhibition constants (K_i).

There is a provision in AutoDock 4.0 to accommodate flexibility in the protein; however, this feature was not used in our study as there are too many flexible basic residues in the binding site that interact with the flexible ligands, such as GAGs. Furthermore, AutoDock tends to take a large amount of time to sample enough conformational space for molecules such as heparin and cyclitols with a large number of degrees of freedom (translational, rotational, and torsional). This can lead to the failure of the scoring function to accurately predict binding affinities. Hence, docking by FRED followed by a Lamarckian genetic algorithm (LGA) search in Autodock were used to determine the key interactions between GAG molecules and CXCL-8.

Molecular Dynamics Simulations. MD simulations were carried out for the CXCL-8 dimer (PDB code: 3IL8, 1IL8) as well as for complexes with the receptor peptide (PDB code: 1ILQ) and the 24-mer heparin fragment. The monomeric CXCL-8 is the relevant form for CXCR1 binding and function, and the monomer coordinates of the dimer structure (PDB code: 1ILQ) were only used for the computational studies of CXCL-8 with the receptor peptide fragment.

Simulations starting with the CXCL-8 NMR and X-ray structures were run at 300, 325, and 337 K for 100 ns each, including an equilibration period of 10 ns. Simulation of the NMR structure was also carried out at 313 K for 100 ns for direct comparison with the NMR determination, which was carried out at 40 °C.²⁶ Simulations were run at different temperatures to investigate if the conformational differences between the NMR and X-ray structures arise due to the influence of thermal motion at higher temperatures. The CXCL-8–receptor peptide and CXCL-8–24mer heparin fragment complexes were also simulated for 50 ns at 308 K. No restraints or constraints were used during the equilibration and production runs for any system, except for the CXCL-8–cyclitol complexes, as described below.

MD simulations were also performed for complexes of CXCL-8 with cyclitols 7, 8, 9, 10, and 10a. During heating and equilibration, distance restraints (with a force constant of 2.0 kcal/(mol Å²)) were applied to all the atoms in the protein that interact with the each ligand to prevent it from leaving the binding site. The CXCL-8–cyclitol complexes were deemed to have equilibrated after 1.5 ns with these distance restraints. The production phases of the simulations (in the absence of any restraints) were then run at 300 K for a further 8.0 ns for the CXCL-8–cyclitol complexes. The trajectories obtained from these simulations were used in the calculation of free energies of binding (see below), for which long simulations are not required.¹⁰⁶

The Parm99SB¹⁰⁷ force field in AMBER 9.0¹⁰⁸ was used for the proteins in all simulations, with the GAFF¹⁰⁹ parameter set used for cyclitols. The GLYCAM06¹¹⁰ parameter set was used for the heparin fragment. Partial atomic charges for cyclitols and the individual units of heparin were obtained using the restricted electrostatic potential (RESP) method¹¹¹ using R.E.D.-III tools.¹¹² Prior to charge derivation, all ligands were subjected to a full quantum mechanics geometry optimization with a HF/6-31G* basis set using Gaussian 03.¹¹³

All energy minimizations and MD simulations were performed with AMBER 9.0.¹⁰⁸ The N- and C-termini of CXCL-8 and the receptor peptide were capped with residues ACE (acetyl beginning group) and NME (N-methylamine ending group), respectively, to remove charges in the end groups. Capping the C-terminus of CXCL-8 was done to further ensure an energetically favorable helix termination. A cubic box of TIP3P water molecules¹¹⁴ was added to solvate the protein and its ligand-bound complexes, keeping a minimum distance of 12.0 Å between each face of the box and the protein. The numbers of water molecules added to the X-ray (PDB code: 3IL8) and NMR (PDB code: 1IL8) structures of CXCL-8 were 9367 and 11899, respectively. In the case of the complex of the CXCL-8 dimer with the receptor peptide (PDB code: 1ILQ), 38518 water molecules were added. The number of water molecules added to the complexes of CXCL-8 with cyclitols 7, 8, 9, 10, and 10a was 9295. The number of water molecules added to the complex of CXCL-8 with a 24-mer heparin fragment was 10758. Net charges in the protein and/or heparin fragments were neutralized by adding an appropriate number of counterions (Na^+ or Cl^-).

Free Energy Calculations. Free energy calculations using the MM/PBSA method have been reported for CXCL-8 homo and heterodimers using the CHARMM force-field.¹¹⁵ We calculated the free energies of binding of cyclitol-CXCL-8 and heparin 24mer-CXCL-8 complexes using the MM/PB(GB)SA method. The MM/PBSA module of AMBER 9.0 was used to compute the above-mentioned components of the free energy. More details of the MM/PB(GB)SA methods can be found in the Supporting Information. For the cyclitol-CXCL-8 complexes, 800 snapshots of the coordinates of the system were taken at 10 ps intervals from the last 8.0 ns of the production runs. For the complexes of CXCL-8 with the 24-mer heparin fragment and the receptor peptide, 1500 snapshots of the coordinates of the systems were taken from the last 30 ns of the simulations. All solvent molecules and counterions were removed prior to analysis. The snapshots were also analyzed with the modified generalized Born (GB) solvation model,¹¹⁶ modified for use with the PARM94 parameters to obtain energies of solvation. Poisson–Boltzmann calculations were also used to obtain solvation energies, with an ionic strength of 0.14 and dielectric constants (ϵ) of 1 for the solute and 80 for the solvent. A probe solvent radius of 1.4 Å and the PARSE atomic radii parameter set¹¹⁷ were used to determine the molecular surface. Different surface parameters were used: in the case of GB calculations, $\gamma = 0.0072 \text{ kcal}/\text{\AA}^2$ and $\beta = 0.0 \text{ kcal/mol}$, and in the case of PB calculations, $\gamma = 0.00542 \text{ kcal}/\text{\AA}^2$ and $\beta = 0.92 \text{ kcal/mol}$.^{117,118}

The vibrational, rotational, and translational entropies of the systems were computed by performing normal modes analyses¹¹⁹ using the Nmode module of AMBER on snapshots collected every 200 ps, resulting in 40 snapshots for the 8.0 ns simulations for various cyclitols complexed with the CXCL-8 dimer. For the complexes of CXCL-8 with the 24-mer heparin fragment and the receptor peptide, snapshots were collected every 500 ps, resulting in 60 snapshots for the last 30 ns of the simulations. Prior to these normal modes analyses, the selected snapshots of the complex, protein, and ligand were subjected to a full conjugate gradients energy minimization using a distance-dependent dielectric ($\epsilon = 4r$) and a convergence criterion of 0.0001 kcal/mol. The reported vibrational, rotational, and translational entropies were calculated as averages over all selected snapshots.

Visualization. All the 3D protein and ligand structures were edited and visualized in Accelrys Discovery Studio 2.1 (Accelrys, Inc.). Consurf results and MD simulation trajectories were

visualized using UCSF Chimera.¹²⁰ The molecular solvent accessible surface area (SASA) and the buried/contacting surface for individual residues were calculated using NOC 3.0¹²¹ with a solvent (water) probe radius of 1.4 Å.

■ RESULTS AND DISCUSSION

Sequence and Structure Analysis. Several studies have been reported for the CXCL-8 family based on a combined sequence, structure, and phylogenetic analysis to understand its structure–function relationship, interpret the evolutionary relationship across family members, understand the receptor specificity exhibited by ligands, locate the functionally important motifs responsible for dimerization, and characterize the relationship between GAG and receptor binding sites.^{65,122–124}

Although multiple sequence alignments (MSA) are a powerful source of information for predicting functional regions in biological sequences, it is necessary to correlate mutation and evolutionary conservation data with the corresponding location in a three-dimensional structure, since residues that are distant in sequence may be found in close proximity in a folded protein. Furthermore, binding surfaces involved in biochemical functions experience different selection pressures from other regions on the surface of proteins.¹²⁵ The Consurf server⁷⁹ and ConSurf-DB¹²⁶ use the 3D-structure of a protein in order to represent such functional regions. In this study the Consurf analysis was carried out using chain A in PDB structure 3IL8 (the PDB numbering of this structure was henceforth used). The MSA that was constructed using the default parameters of the ConSurf DB server contained 50 homologues, which include CXCL-4, 5, 6, 13, 15, and 19 family ligands as well as PF4 (platelet factor 4). The fish analogues of CXCL-8 are not included in the hit list after searching ConSurf DB with default PSI-BLAST parameters. Consequently, a query with the CXCL-8 structure using default parameters in ConSurf DB results in the incorrect assignment of conservation scores for the majority of residues (Supporting Information Figures S2 and S3).

In order to study the phylogenetic relationships between the distinct members of the CXCL-8 family, the MSA of the 39 CXCL-8 sequences listed in Supporting Information Table S1 was constructed using MUSCLE [62]. The ELR motif, residues in the second β -sheet and the cysteine residues involved in disulfide bridges, appear to be highly conserved in both default Consurf and manually curated analyses (Supporting Information Figures S2 and S3 and Figure 2). The ELR motif has been substituted with other amino acids in *Chimaera phantasma*, *Paralichthys olivaceus*, *Latris lineata*, and *Latris lineata* (Supporting Information Figure S4). Residues His18 and Lys20 showed conservation scores of 4 and 6, respectively, upon inclusion of CXCL-8 sequences from fish. There was an additional serine found in the second β -sheet of *Dasypus novemcinctus* (Supporting Information Figure S4). Residues in the first β -sheet which form the dimer interface appear to be only partially conserved based on the Consurf analysis of the CXCL-8 monomer structure. Analyses using both methods suggest that residues in the third β -sheet and the GAG binding site in the C-terminus are highly variable. Residues Arg60 and Lys64 both had a conservation score of 1, while Lys67 and Arg68 had conservation scores of 3 and 4, respectively. Consequently, it appears that human CXCL-8 may have unique features that distinguish it from chemokines expressed in other species with respect to interactions with molecules at the cell-surface, such as sulfated GAGs.

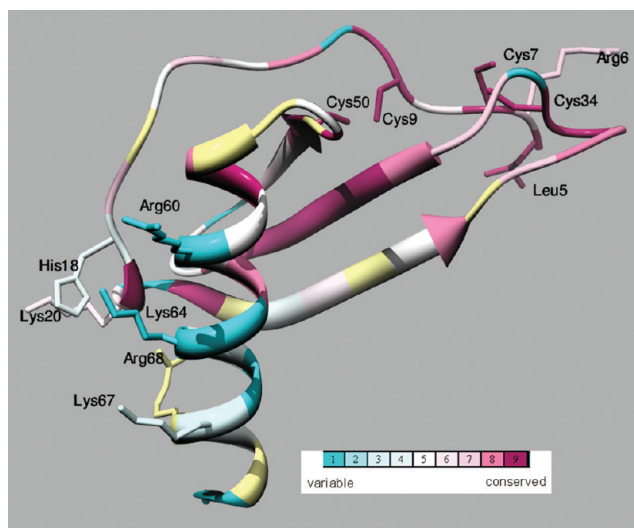


Figure 2. Representation of the structure of CXCL-8 (PDB code: 3IL8) upon multiple sequence alignment with other known CXCL-8 proteins. The structure is colored according to the Consurf color schemes, from turquoise to burgundy, representing evolutionary conservation scores from variable through conserved.

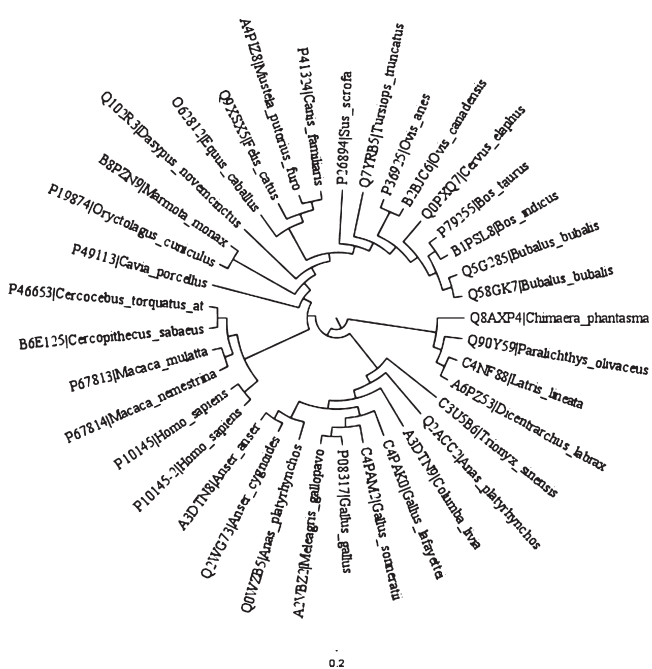


Figure 3. Polar phylogenetic trees of CXCL-8 sequences computed from a multiple sequence alignment using MUSCLE. The phylogenetic tree produced by Consurf was plotted using FigTree 1.2.2.⁸⁰

A molecular phylogenetic tree was constructed to analyze the evolutionary relationships of CXCL-8 proteins (Figure 3). Sequence homology reveals that human CXCL-8 is very closely related to macaque, and hence, they are clustered on the same clade (Figure 3). The CXCL-8 encoding region of fish species *Chimaera phantasma*,¹²⁷ *Paralichthys olivaceus*,¹²⁸ *Latris lineata*,¹²⁹ and *Dicentrarchus labrax*¹³⁰ is clustered into one lineage. The CXCL-8 sequences of the fish species studied lack the ELR motif which, in humans, induces a chemotactic effect on neutrophils and an angiogenic effect,¹⁵ suggesting that CXCL-8 may not possess these

functions in fish. These results also suggest that avian CXCL-8 proteins evolved distinctly from those of mammals.¹³¹ In this study, we undertook an evolutionary survey of sequence substitution patterns of CXCL-8 but not its receptors. The evolutionary analyses of chemokines and their receptors have already been reported,^{132–135} suggesting that as the N-terminus and transmembrane portions of chemokine receptors are involved in ligand/receptor binding and recognition, amino acid substitutions in the N-terminus of the receptor as well as in the ligands in various species could potentially modify the ligand–receptor interaction, i.e., the specificity and/or affinity as compared to human CXCL-8/CXCR1 interactions. For example, the mouse CXCL-8 receptor does not bind human CXCL-8 with high affinity.¹³⁶ Such divergence may have resulted in important differences in the function of chemokines between species.

The electrostatic potential of proteins arising from charged sidechains plays a role in protein folding and stability and specific protein–protein/ligand recognition. In general, electrostatic surface representation aids in the prediction of protein–ligand interactions based on the concept of charge complementarity. Supporting Information Figure S5 shows the electrostatic surface representation of CXCL-8 using its X-ray structure (PDB code: 3IL8). Positive electrostatic potential surfaces are shown in blue, and negative electrostatic potential surfaces are shown in red. A positively charged area of the protein surface can be seen to be created by the C-terminal α -helix together with the loop connecting the extended N-terminal strand region with the first β -strand of the sheet, wherein the basic residues alongside the alpha helices can interact with negatively charged ligands like heparin. In this study, CXCL-8 is taken to be at acidic pH, wherein all histidines are considered protonated.¹³⁷

Sulfate Binding Motif Search. Various approaches have been used to identify heparin/GAG-binding sites on the surface of proteins. These have been based on amino acid composition,^{138,139} consensus sequences,¹⁴⁰ secondary structure,¹⁴¹ spatial distribution of basic amino acids,¹⁴² and the electrostatic surface properties of proteins.¹⁴³ GAG-binding sites generally consist of a cluster of basic residues on the protein surface but not necessarily in a continuous sequence. A survey of sulfate-binding regions from the PDB database can reveal several positively charged regions on a protein surface which might form the binding site of sulfated GAGs.⁸⁶ In this work, the PDB database was surveyed for sulfate-binding motifs using SSM searches to look for proteins with a similar fold as CXCL-8 and that have been crystallized with sulfate ions or sulfated ligands. The mutant structure of the CXCL-8 dimer (PDB code: 1QE6)³⁰ was crystallized with two sulfates: one located near residues Ser1 and Arg6 in the N-terminus and another one located near residues His18, Pro19, and Lys20. Table 3 lists details of different structural homologues of CXCL-8 along with their sulfate binding regions. It appears that most of the sulfates and sulfated ligands could be mapped to residues in the vicinity of His18, Lys20, Lys64, and Arg68 of the C-terminal helix. One of the examples is shown in Figure 4A. These residues are indeed already known to play an important role in heparin binding.⁵⁷ In addition to the heparin binding regions present on CXCL-8, we found sulfate-binding motifs in the vicinity of Arg47, which suggests that this residue may further extend the length of the putative heparin binding site.

Some of the sulfated ligands complexed with structural homologues of CXCL-8 were found to be associated with residues on the β -sheet surface of CXCL-8. One of these structural homologues is CXCL-12 (PDB code: 2NWG), bound with two heparin disaccharides. One of the disaccharides would

Table 3. Prediction of Sulfate Binding Motifs

PDB code	protein	amino acids of target structures involved in sulfate binding with reference to the CXCL-8 structure (indicated in bold)			rmsd (Å) calculated between the Cα-atoms of matched residues in the best 3D superposition of the target structures and the reference CXCL-8 structure (1QE6)	% sequence identity between the target and CXCL-8	% structural structure element match of the target protein with respect to the CXCL-8 structure (1QE6)
1F9P	connective tissue activating peptide- III (CTAP-III)	His35 His18 Arg 20 Asn30 Glu29 His25 Glu24 Arg41 Lys42	Pro36 Pro19 Ala19 Lys64 Phe17 Lys20 Lys64 Arg68 Lys27 Asn45 Arg26	Lys 81 Lys64 Ala21 Lys20 Lys64 Arg68 Lys27 Asn45	1.28	35	64
2NWG ¹⁷⁵	stromal cell-derived factor-1alpha/CXCL-12 (SDF-1α)				2.65	29	100
1QG7 ¹⁷⁶ , 1A15 ⁸³		Ala19 His18	Arg20 Pro19	Ala21 Lys64	2.70	22	100
2HCl ¹⁷⁷	human macrophage inflammatory protein-3alpha (MIP-3α)	Leu15 Phe17 Thr54 Gln56 Cys32 Cys34 Pro51 Val67 Pro53 Ala69 Gly31 Ala28 His33 Ser30	Trp55 Trp57 Trp55 Trp57 Gln53 Glu55 Gln26 Glu29 Leu27 Ile28 Ile37 Asn35 Glu29 Ile39 Thr37 Asp33 Cys32 Ala35 Cys34		1.71	27	80
2RA4 ¹⁷⁸	human monocyte chemoattractant protein 4 (MCP-4/CCL-13)	Arg24 Phe21 Lys18 His18 Lys48 Arg47	Lys18 Lys15 Ser21 Pro19 Thr44 Leu43	Lys48 Arg47 Arg24 Phe21 Arg24 Phe21	1.6	29	80
1B3A ¹⁷⁹	anti-HIV protein aop-rantes	His23 Lys45	Arg47 Arg44	Thr43	1.76	23	80
1EQT ⁸⁵	Met-rantes	Phe21 Asp45	Arg47 Ser44	Leu43			
1U4R ¹⁸⁰	human rantes mutant 44-aana-47	Ser31 Glu29 Phe28 Arg26	Gly32 Ser30 Pro9 Cys7	Lys33 Cys33	1.59 1.96	21 19	80 80

be superimposed near His18 and Lys20 of CXCL-8, whereas the other heparin disaccharide binding site consists of a BBXB motif (in this case Lys-His-Leu-Lys) in the 40s loop near the dimerization interface connecting the two β -sheets. There are several reasons why it is unlikely that a heparin saccharide can bind to CXCL-8 on the β -sheet surface. First, the histidine in the BBXB motif of CXCL-12 has been substituted by Glu in CXCL-8 (Figure 4B). Second, superimposition of the backbone of CXCL-12 onto that of CXCL-8 using a SSM search results in a rmsd greater than 2.5 Å, with a larger deviation in the sulfate binding motif region. Third, the CXCL-8 dimer displays the same positively charged area on the surface of the α -helices, except in the SDF-1 α dimer, where the highest positively charged area is on the back of the β -sheet formed by the dimer interface, as reported before using a cluster analysis of chemokine iso-surfaces.⁶⁵ CXCL ligands such as macrophage inflammatory protein-3alpha (MIP-3 α) and RANTES bind sulfates and sulfated ligands in the region formed by a long loop connecting the third β -strand and the C-terminal α -helix. However, due to the

lack of proper sequence identity in the β -sheet regions on the target and CXCL-8 structures, it is not possible to establish a correlation with the sulfate binding region. Human monocyte chemoattractant protein 4 (MCP-4), which makes a CC type of dimer, displays an arrangement of sulfates similar to the CXCL-8 cluster.

MD Simulations of the Complex of CXCL-8 with the Receptor Peptide Fragment. We have also aimed to characterize the interactions of the extracellular fragment of the CXCR-1 receptor, one of the binding partners of CXCL-8, and its associated conformational changes using MD simulations to try to provide the basis for the future structure-based design of chemokine antagonists.

Recent NMR determinations show that the N-terminal domain of the receptor interacts with the entire N-terminal of CXCL-8 through a combination of polar, electrostatic, and hydrophobic/packing interactions and that this binding triggers propagated conformational changes throughout CXCL-8 required for binding affinity and function,⁵⁵ in contrast to previous

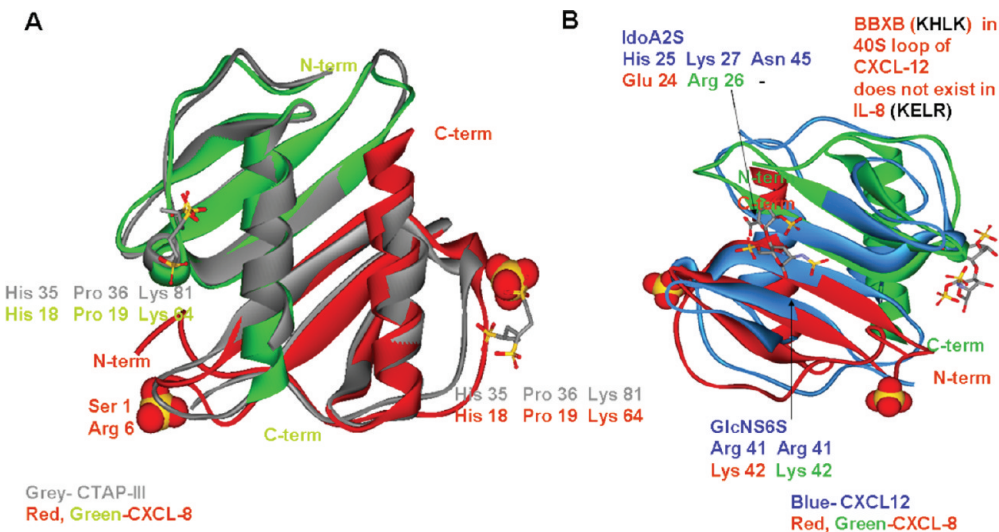


Figure 4. Example of sulfate binding motifs mapped on the CXCL-8 structure 1QE6 based on the superimposition of the target structures (A) CTAP-III and (B) CXCL-12, as obtained by SSM search. Corresponding residues in the target structures are aligned with reference to amino acids in CXCL-8. The protein surface created by the C-terminal α -helix together with the loop connecting the extended N-terminal strand region with the first β -strand of the sheet can interact with sulfates and sulfated ligands. It does not appear possible for a heparin saccharide to bind to CXCL-8 on its β -sheet surface.

suggestions that a subset of highly clustered hydrophobic N-loop residues defines the binding region.^{23,144} Furthermore, the N-termini of the receptor peptide and CXCL-8 show characteristics of unstructured or minimally structured domains and hence can form a larger binding region than the folded protein with its restricted conformational freedom. In order to better understand the dynamical behavior of the complex of CXCL-8 with the receptor peptide, we performed unrestrained MD simulations starting with the reported minimized mean NMR structure (PDB code: 1ILQ) of the synthetic receptor peptide (referred to as RP hereafter) and CXCL-8 (Figure 5A), wherein Pro9 and Pro10 of the RP interact with Tyr13, Phe17, Phe21, Leu43, Arg47, and Leu49 of CXCL-8, and Tyr15 of the RP has contacts with Ile10, Lys11, Tyr13, and Leu49 of CXCL-8.²⁵ In addition to hydrophobic contacts, the ensemble of structures of the RP (PDB code: 1ILP) suggested the presence of intermolecular charge–charge interactions between Asp12, Glu13, and Asp14 of the RP and Lys15, Arg47, and Lys11 of CXCL-8, respectively.

Residues Pro9 and Pro10 of the RP retain their interactions with Tyr13, Tyr15, Phe21, and Arg47 during the MD simulations. Calculations of the SASA and buried surface for individual residues suggested that residues Phe17, Pro19, Ile22, Val27, Ile28, Ile39, Val41, Leu49, Val61, Val62, Phe65, and Ala69 of CXCL-8 are buried. Buried residues Phe17 and Leu49 were not directly involved in interactions with the RP during the simulations, which is consistent with a structural model recently proposed.⁵⁵ The intermolecular charge–charge interactions between Glu13 and Asp14 of the RP and Arg47 and Lys11 of CXCL-8, respectively, were observed during the MD simulations; however, the ionic interaction between Asp12 of RP and Lys15 of CXCL-8 were not observed.

Visualization and DSSP analyses of trajectories showed that residues Met1 to Met8 of the RP retained their disordered secondary structure during the MD simulations, consistent with the NMR-determined structural ensemble (Figure 5B). In the initial structure (prior to the production stage of the simulations), the side-chain of Asp5 of the RP makes a salt bridge with Lys20 of CXCL-8. The electrostatic interactions between the side-chain of

Asp5 with the N ϵ 1 of His18 of CXCL-8 were observed throughout the production run while the transient electrostatic interactions between the side-chain of Asp6 of RP and the side-chain of Lys64 located in the C-terminal helix of CXCL-8 were observed after 44 ns (Figure 5C). Studies of C-terminus deletion mutants and a CXCL-8 chimera containing helices suggested that the C-terminal α -helix is not directly involved in CXCL-8 receptor binding but helps to stabilize the tertiary structure.^{21,145} In contrast, the flexible N-terminus of the RP was found to interact with residues of the C-terminal helix of CXCL-8 during MD simulations. This mechanism of interaction is similar to the one observed in HLA-A2, a structural homologue of CXCL-8, where the antiparallel C-terminal helices of the dimer form the receptor binding site.²⁶ The nitrogen in the pyrrolidine ring of Trp2 and the backbone carbonyl of Pro10 from the RP make hydrogen bonds with the backbone carbonyl group of Asn71 and the side-chain of Arg47 of CXCL-8, respectively. The hydrogen bond between Trp2 of RP and Asn71 is detected only after 45 ns during the simulation (Figure 5C). In our simulations, a hydrogen bond is also observed between the backbone carbonyl of Tyr15 of the RP and the backbone NH of Cys50 of CXCL-8, suggesting that it plays an important role in receptor binding, as reported in a study of synthetic CXCL-8 analogues.²¹ The interactions of Pro17 at the C-terminus of the RP with Gln8, Ile10 and Ile40 of CXCL-8 were retained during the simulations. The interaction between the sidechain of the amine capping residue of the RP with the backbone of Gln8 of CXCL-8 was also retained during the simulation. The time evolution of the backbone rmsds of the whole CXCL-8 dimer, the C-terminal helices of CXCL-8, and the RP fragment are shown in Supporting Information Figure S6, wherein the largest rmsd contribution comes from the flexible RP. The conformation of the C-terminus of the RP is preserved throughout the simulation. MD simulation of the CXCL-8-receptor fragment complex suggest similar conformational changes throughout the CXCL-8 protein (as discussed below in the simulations of the CXCL-8 dimer) and the bound receptor peptide, and also reveal aromatic, hydrophobic, and electrostatic interactions between CXCL-8 and the receptor fragment. These interactions might further be explored for the rational design of novel peptides which

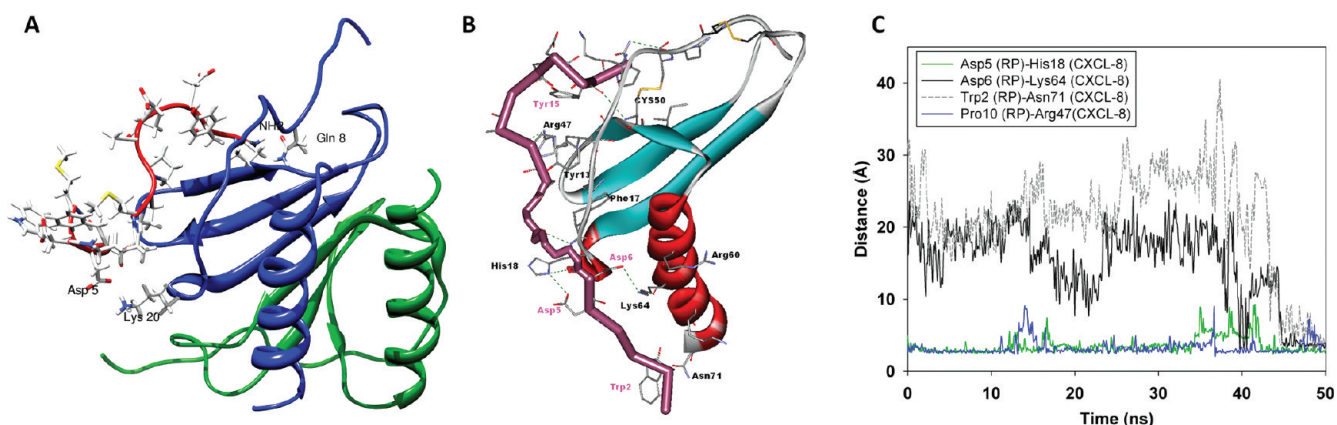


Figure 5. (A) NMR structure of wild-type CXCL-8 in complex with a peptide analogue of CXCR1. The NMR structure reveals the interaction of the receptor peptide and CXCL-8 to be primarily hydrophobic. Two hydrogen bonds are present. The sidechains of Asp5 and the amine capping residue NH₂ of the receptor peptide make hydrogen bonds with Lys20 and Gln8 of CXCL-8, respectively. (B) Snapshot taken from the 50 ns simulation of the CXCL-8–receptor peptide complex. The interactions are highlighted by green dotted lines. The peptide is represented by sticks in magenta, and the CXCL-8 structure is shown according to secondary structure. Only a few residues and monomer of CXCL-8 are shown for clarity. The labels in black indicate residues from the CXCL-8 structure, and the labels in magenta correspond to the synthetic peptide. (C) Plot of the distance between the interacting residues of receptor peptide and CXCL-8. The electrostatic interactions between the sidechain (carboxyl atoms) of Asp5 with the Nε1 of His18 of CXCL-8 were observed throughout the production runs. The electrostatic interactions between sidechain (carboxyl atoms) of Asp6 of RP and sidechain (nitrogen atom) of Lys64 located in the C-terminal helix of CXCL-8 and the hydrogen bond between nitrogen in the pyrrolidine ring of Trp2 of RP and backbone carbonyl of Asn71 of CXCL-8 were transient. The hydrogen bond between backbone carbonyl of Pro10 from RP and the sidechain of Arg47 of CXCL-8 was also observed over the course of the trajectory.

can inhibit formation of the protein complex and serve as a model for the structure-based design of small-molecule analogues to treat inflammatory diseases.

Binding-induced dissociation studies of a trapped disulfide-linked dimer and the wild-type dimer indicated that binding to the receptor N-terminal domain induces dissociation of the dimer–receptor complex into a monomer–receptor complex due to conformational flexibility and that the receptor-bound dimer is thermodynamically unfavorable while the receptor-bound monomer is the favored state.⁵⁵ In our MD simulations, we could not observe any disruption caused by the N-terminal receptor peptide at the dimer interface, which has extensive H-bonding and packing interactions. It is possible, however, that upon dissociation more residues from CXCL-8 become available to interact with the negatively charged N-terminus of the RP, making the monomer a high-affinity ligand for the CXCR1 receptor.

The free energies of binding predicted from a 30.0 ns MD simulation trajectory using the MM/PB(GB)SA method are reported in Supporting Information Table S2. Large changes in the free energies can be attributed to either solvation effects or electrostatic effects. The change in free energy is dominated by the electrostatic component as opposed to hydrophobic interactions. This is due to the presence of a large number of charged residues (Lys11, His18, Lys20, Arg47, Lys64) of CXCL-8, which provide a sufficient number of electrostatic interaction partners for the receptor peptide. These in silico binding energies cannot be compared quantitatively to experimentally obtained dissociation constant (K_d) values²⁵ but can be useful to evaluate the relative binding affinities of mutant peptides that may become available in the future. Recently, an empirical approach using the all-atom free-energy force-field PFF02^{146,147} was employed to analyze the influence of mutations on the complex of CXCL-8 with the N-terminal peptide of its cognate receptor CXCR1.¹⁴⁸ Seventeen of the individual residues of the N-terminal peptide of CXCR1 receptor were mutated to alanine. Mutations in Met1, Trp2, Gly7, Met8, Pro9, Pro10, Tyr15, Ser16, and Pro17 were shown to have little

effect on the interaction energy. In contrast, substantial changes in the interaction energy were seen with substitutions in most of the charged amino acids: Asp3, Phe4, Asp5, Asp6, Asp12, Glu13, and Asp14, the largest being for Asp12. Those calculations were carried out keeping the chemokine backbone rigid while the RP was annealed within its binding region, resulting in an energy-optimized conformation that had a 2.25 Å rmsd from the experimental structure. These results cannot be directly compared with our MD simulations using the MM/PB(GB)SA method because of the fluctuations in the complex and high flexibility in the N-terminus of the RP (rmsd greater than 4 Å), whereas the above Monte Carlo free energy simulations neglect the entropic contributions. Empirical bioinformatics approaches and the MM/PB(GB)SA method benefit from their computational efficiency but are not the methods of choice when large conformational changes in proteins are involved.¹⁴⁹ Consideration of structural flexibility may be better treated through the use of structural ensembles, as in the CC/PBSA method.¹⁵⁰

MD Simulations of the CXCL-8 Dimer. Earlier 1.0 ns long NVE MD simulations at 300 K of the NMR-determined structure of CXCL-8 using explicit and implicit solvent models predicted the relative motion of the antiparallel α -helices in the dimer.⁴¹ The continuum solvent simulation showed slightly larger deviations from the initial NMR-determined structure, but in general, the implicit and explicit solvent simulations similarly predicted the relative approach of the α -helices, making the structure similar to that determined by X-ray diffraction. These simulations may not have been either long enough to capture the alternating conformational behavior of the α -helices in the CXCL-8 dimer and predict with accuracy a realistic interhelical distance. Moreover, the NMR structure was determined at an acidic pH at 313 K. Consequently, we have performed NPT MD simulations of the CXCL-8 dimer starting with the NMR-determined structure at 300, 313, 325, and 337 K for 100.0 ns with all histidines protonated. Simulations starting with the X-ray structure of CXCL-8 were carried out at 300, 325, and 337 K

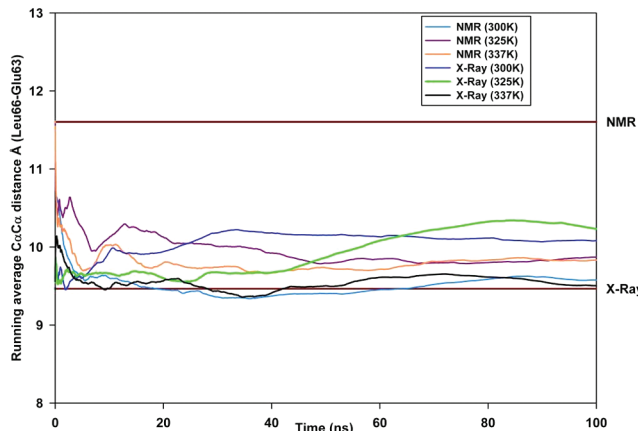


Figure 6. (A) Plots of the running averages of the distance between the C α atoms of Leu66 on one monomer and Glu63 on the other monomer. The structure of the CXCL-8 dimer was taken from X-ray and NMR structures and was simulated at different temperatures. The reference lines are shown to indicate the reference initial conformations having C α –C α distances of 9.47 Å (X-ray) and 11.61 Å (NMR). The coordinates of the CXCL-8 dimer were taken from X-ray and NMR structures and were simulated at different temperatures.

under the same conditions. These simulations were aimed at investigating the interhelical dynamics.

The distance between residues Leu66 of one monomer and Glu63 of the other is approximately 9.47 Å in the X-ray structure and 11.61 Å in the NMR structure. Analysis of the structures in the NMR-determined ensemble (PDB code: 2IL8) revealed an interhelical distance ranging from 11.0 to 12.74 Å. This interhelical distance was monitored during each of our simulations and the running averages are plotted in Figure 6. Although the interhelical distance would be expected to be similar to the one observed in the NMR structure in solution, the simulations in explicit water at different temperatures show that the interhelical distance did not converge to a value close to 11.0 Å. Simulations of the NMR structure at 300 (Figure 6) and 313 K (not shown) reveal that the interhelical distance closely resembled that observed in the X-ray structure. MD simulations at higher temperatures (325 and 337 K) also showed the two antiparallel helices moving closer together and reaching a distance of 9.87 Å, whereas simulations starting from the X-ray structure at 300 and 325 K showed the two helices moving further away from each other. The interhelical distance of the X-ray structure at the end of the simulation at 337 K was close to the initial starting distance of 9.5 Å. This high temperature simulation suggests that increased sampling (as achieved by using a higher temperature or by running a significantly longer simulation) results in a dynamic interhelical distance that nonetheless tends to converge to the distance found in the X-ray structure.

While it is possible to consider alternative measurements of the interhelical distance between equivalent positions along the length of the helices, we considered the distance between residues Leu66 of one monomer and Glu63 of the other for consistency with previous simulations.⁴¹ The interhelical distances between equivalent positions along the length of the helices measured using the Interhlx program¹⁵¹ were found to be 13.7 and 17.5 Å in the initial X-ray and NMR structures, respectively, which converged to 11.76 (X-ray) and 13.19 Å (NMR) at the end of our simulations at 300 K. Regardless of

the choice of interhelical pairs, it is clear that the interhelical distance measured in the NMR structure during the simulations resembled the interhelical distance observed in the X-ray structure.

The relative orientations of the α -helices with respect to each other were measured using the Interhlx program.¹⁵¹ The interhelical angles (tilt angle between two different helices) were found to be similar: 165.48° and 169.0° in the initial X-ray and NMR structures, respectively. The average interhelical angles at the end of the simulations at 300 K were found to be 159.40° and 167.0° for the X-ray and NMR structures, respectively.

Nuclear Overhauser effect (NOE) restraints involving residues in the region 23–36 and the C-terminal helices were significantly different from those expected in the X-ray structure of the CXCL-8 dimer.^{28,152} This difference in the region 23–36 is, however, of secondary importance for determining receptor binding specificity⁶³ because the specificity resides in the N-loop region of CXCL-8. The differences in the interhelical region could nonetheless be exploited for the design of inhibitors. Our simulations suggest that the interhelical distance in the X-ray structure can be used to model interactions with molecules such as cyclitols (see further below).

The rmsds of all atoms, backbone atoms, and backbone atoms of the helices and the N-terminus were monitored in each of the simulations of dimeric CXCL-8. The average rmsd of all backbone atoms of the CXCL-8 dimer in MD simulations starting from the X-ray structure was consistently smaller than in the simulations starting from the NMR structure (Figure 7A). The monomers within the dimer were also found to be relatively stable with RMSDs, not exceeding 3.0 Å during the 100 ns runs (Figure 7B). We also monitored the distance between the backbone NH of Gln8 and the N ε atom of His33 in both the NMR and X-ray structures of the CXCL-8 dimer, as reported in previous MD simulations.⁴¹ ^1H NMR spectroscopy has confirmed the presence of a hydrogen bond between the backbone amide of Gln8 and Cys9 and the carboxylate in Glu38; however, these interactions, although present in the N-terminus, are not relevant for neutrophil activation.^{153,154}

Findings from both our MD simulations and those earlier reported⁴¹ rely on the accuracy of the force fields used. Use of the AMBER force field ff94¹⁵⁵ (as used in the earlier MD study of CXCL-8)⁴¹ and its variants¹⁵⁶ is known to lead to the over-stabilization of helical systems and the adoption of stable helices for sequences that have been experimentally determined not to have helical structures.¹⁵⁷ On the other hand, use of the AMBER ff96 force field has been observed to overestimate β -strand propensity.¹⁵⁸ AMBER ff99SB, used in this study, is known to have some limitations for the modeling of the sidechains of Ile, Leu, Asp, and Asn in helical peptides.^{159–161} Nevertheless, other works have shown good agreement between simulations using ff99SB and NMR structural and relaxation data compared to other AMBER variants,^{89,160,162,163} making it an appropriate choice for this work.

Changes to the secondary structure of the CXCL-8 dimer during the simulations were also monitored to help to identify the region which contributes the most to the conformational flexibility of this structure. This analysis was carried out using the DSSP method of Kabsch and Sander¹⁶⁴ for every snapshot collected every 500 ps, as discussed above, monitoring the simulations at 300 K starting from both the NMR and X-ray structures, and is shown in Supporting Information Figures S7 and S8, respectively. The results were mapped onto the corresponding 3D-structures, as shown in Figure 8, where the regions

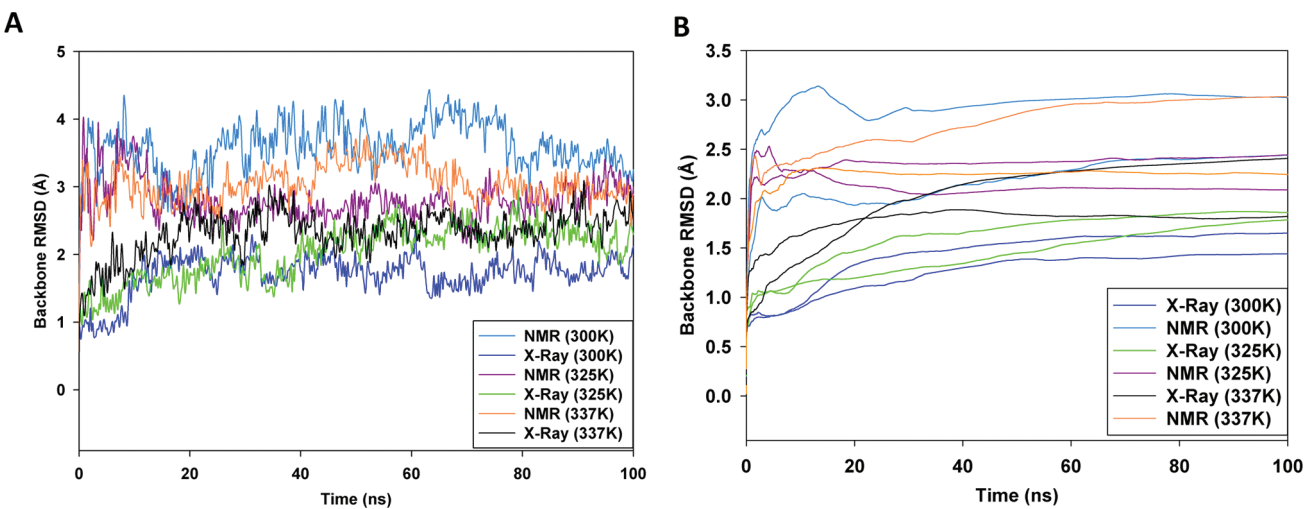


Figure 7. (A) Backbone average rmsd of the CXCL-8 dimer at different temperatures in simulations starting with the NMR and X-ray structures. All backbone rmsd in MD simulations starting from the X-ray structure were consistently smaller than those starting with the NMR structure. (B) Backbone average rmsd of the individual monomers present in the CXCL-8 dimer at different temperatures in simulations starting with the NMR and X-ray structures.

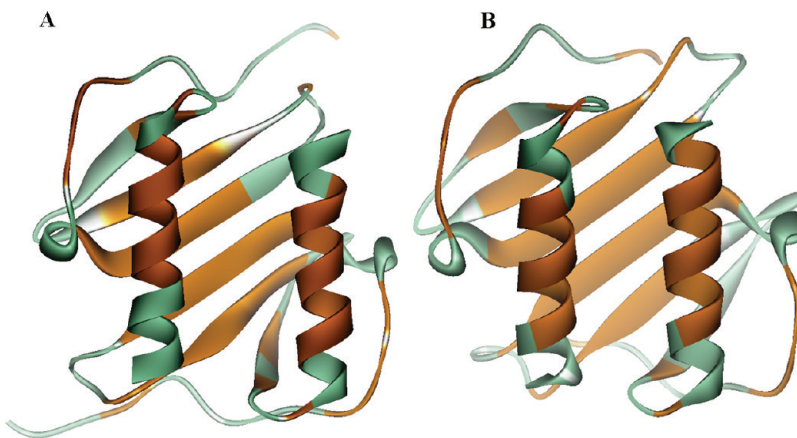


Figure 8. DSSP analysis monitored during 100 ns simulations at 300 K starting from (A) NMR and (B) X-ray structures mapped on the CXCL-8 3D structure. The regions which experience significant conformational change during the MD simulations are shown in cyan. The regions that preserve their conformation are shown in gold. Significant changes in the secondary structure are observed in the N-terminal loop, the β -sheet, and the C-terminal helices. The secondary structure of β -sheets connecting the two monomers were dynamically conserved during the simulations.

that experience significant conformational changes during the simulations are shown in cyan and the regions that preserve their conformation are shown in gold. The secondary structure of the β -sheets connecting the two monomers was “dynamically” conserved during the simulations, most likely due to the presence of intermolecular hydrogen bonds. Significant changes to the secondary structure were observed in the N-terminal loop, the β -sheet, and the C-terminal helices. This suggests that flexibility in the CXCL-8 dimer can be attributed to the concerted rather than independent motions in regions of secondary structure, as reported previously.¹⁶⁵

NMA was used to analyze the motions of the α -helices in the NMR and X-ray structures of the CXCL-8 dimer. The low frequency, high amplitude vibration modes characterized by this approach were used to reveal the large scale movements associated with the relative motion of the two monomers. The output of these calculations in PDB format corresponding to the sixteenth and eighteenth lowest frequency modes are provided in the Supporting Information as c1003366_si_002.pdb and c1003366_si_003.pdb. These modes were selected because they exhibited the highest degree of collectivity, as a measure of the fraction of residues that are significantly affected by a given vibrational mode. Visual inspection of these vibrations revealed that the conformational flexibility in the β -sheet accompanies the shearing movement in the C-terminal helices. This is consistent with our previous analysis of changes to the secondary structure during the MD simulations. On the basis of the results of our MD simulations and secondary structure and NMA analyses, it seems reasonable to propose the existence of shearing movements in CXCL-8 and, in particular, low-frequency conformational

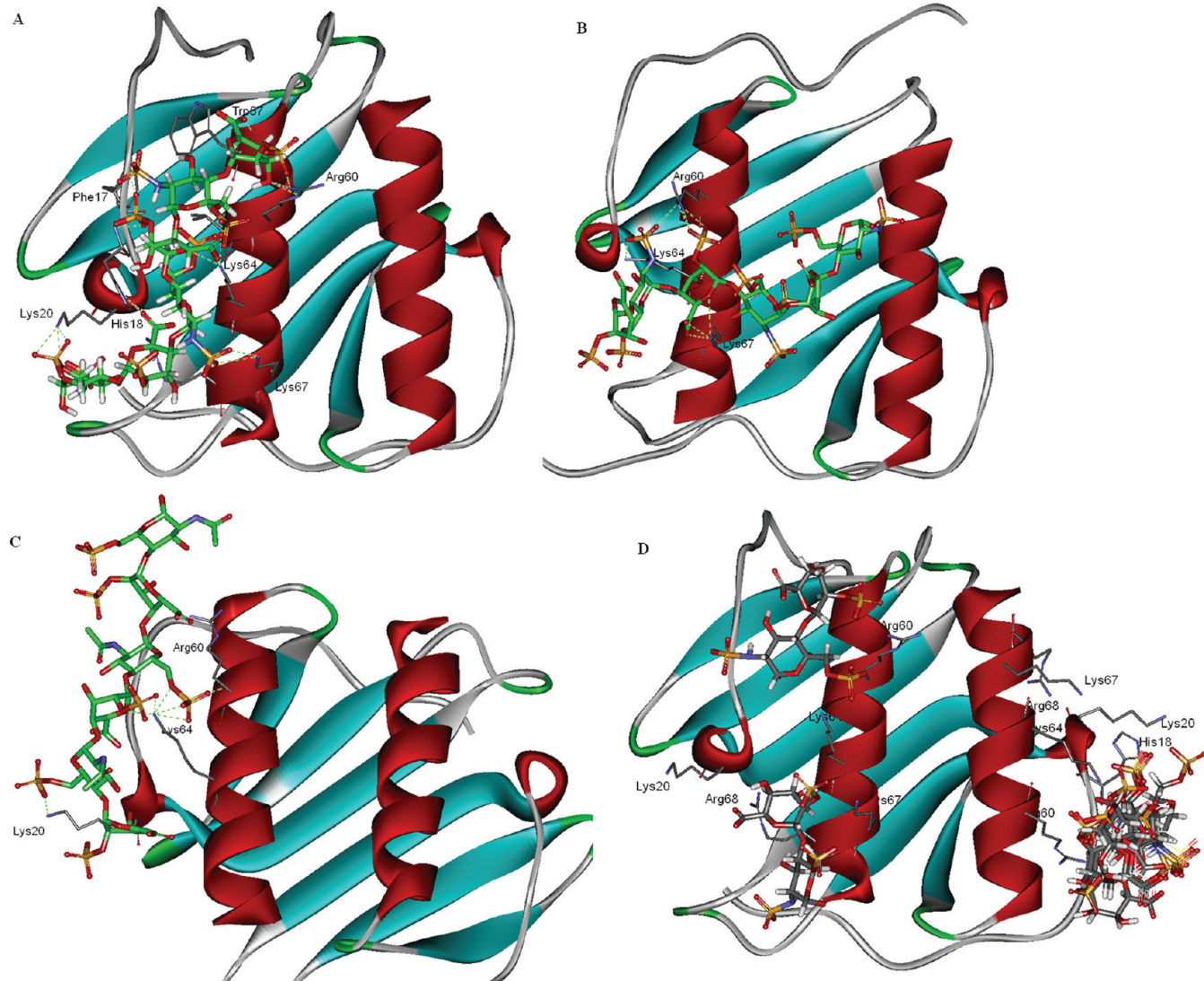


Figure 9. Binding mode and interactions of heparin with CXCL-8 predicted by docking simulations. Interacting residues are represented as sticks. (A) Interaction of Heparin H1 parallel to the C-terminal helical axis. (B) Interaction of Heparin H1 perpendicular to the C-terminal helical axis. (C) Interaction of Heparin H2 with the CXCL-8 monomer, indicating that O-sulfation is important for binding. (D) Cluster of docked conformations of disaccharide H9 observed on the GAG binding surface of CXCL-8, indicating the presence of a multivalent binding mode.

motions in the C-terminal helices. This conformational behavior might be exploited for the rational design of inhibitors bridging the dimer structure of CXCL-8.

Molecular Docking of Heparin Fragments. Free energy calculations using the MM/PB(GB)SA approach have also been successfully used to rank the relative binding affinities of several glycan–protein complexes.¹⁶⁶ However, MM/PB(GB)SA calculations are known to overestimate the free energies of binding of heparin–protein complexes¹⁶⁷ as none of the current PB or GB implicit solvation methods have been developed to specifically treat the desolvation energies and polarization effects arising from the polyanionic nature of GAGs. Studies have shown that AutoDock is effective in studying the docking of highly charged large molecules such as GAGs.^{66,86} Consequently, docking of the heparin analogues reported in Table 1 was considered to be a more feasible approach to predict free energies than MM/PB(GB)SA. These analogues were blind docked (site 3) to the whole surface of CXCL-8. During the docking simulations, clustering of docked poses at site 1 (parallel to

the helical axis in the monomers) and site 2 (perpendicular to the helical axis in the dimer) were observed (Figure 9A and B). The interactions of various heparin analogues with CXCL-8 and the binding affinities predicted by AutoDock for the lowest energy poses are reported in Table 4.

Previous docking simulations reported that the lowest energy conformation of a heparin hexasaccharide has a perpendicular orientation and bridges the gap between the two antiparallel α -helices.⁶⁶ A consistent set of residues (His18, Lys20, Lys64, Lys67, and Arg68) were identified as possible interaction partners for the heparin oligosaccharides in our docking simulations. In contrast to the previous study,⁶⁶ all the low energy conformations of sulfated heparin were observed to cluster parallel to the C-terminal helical axis of the X-ray structure of CXCL-8 (Figure 9). No docking simulations were performed with the NMR structure of monomeric CXCL-8 (PDB code: 1IKL), where the amide of Leu25 was modified into N-methyl (L25NMe).²⁷ The main difference between this monomer and

Table 4. Docking of Heparin Fragments to CXCL-8^a

heparin no.	AutoDock energy of binding (kcal/mol)	K_i	lowest energy binding modes	interactions with residues of CXCL-8 within 3.5 Å
H1	-10.19	33.82 nM	parallel	sidechains of His18, Lys20, Arg60, Lys64, Lys67, and Arg68, backbone of Phe17 and Trp57
	-4.72	346.62 μM	perpendicular	sidechains of Arg60, Lys64, and Lys67
H2	-8.41	681.43 nM	parallel	sidechains of Lys20, Arg60, and Lys64
H3	-3.99	1.19 mM		sidechains of Arg60, Lys64, backbone of Pro16, Phe17
H4	-4.03	1.11 mM		sidechain of Arg60, backbone of Phe17
H5	-3.33	3.65 mM	parallel	sidechains of His18, Arg60, Lys64, and Arg68
H6	-4.58	438.21 μM	parallel	sidechains of His18, Arg60, and Lys64, backbone of Arg68
H7	-5.82	54.09 μM	parallel	sidechains of His18 and Lys64
H8	-3.26	4.07 mM		backbone of Pro16 and Phe17
H9	-4.89	259.67 μM		sidechains of His18, Lys20, Arg60, Lys64, Lys67, and Arg68
H10	-4.41	587 μM		sidechain of Lys 64 or sidechain of Arg47
H11	-4.25	763 μM		sidechain of Glu63
H12	-4.26	754 μM		sidechain of Glu63

^a Parallel binding mode: heparin axis is parallel to the C-terminal helical axis of CXCL-8. Perpendicular binding mode: heparin axis is perpendicular to the C-terminal helical axis of CXCL-8.

the X-ray and NMR structures of the dimer is in the GAG-binding site in the C-terminal helix, which leads to significant differences in the results of docking.

In this present study, docking simulations of a heparin disaccharide resulted in many binding pose clusters in the vicinity of basic residues, suggesting that heparin disaccharides can bind the CXCL-8 monomer or dimer in multivalent mode. Heparin hexasaccharides H1 and H2 were predicted to make the majority of their interactions with the heparin binding site (basic residues Lys20, Arg60, and Lys64) through their O-sulfate groups (Figure 9A and C), whereas the *N*-acetylated group was not found to interact with the heparin binding site. Hence, on the basis of these docking simulations of the two heparin hexasaccharides reported here, it seems that O-sulfation is more important than N-sulfation for the binding to CXCL-8, consistent with experimental data.⁵⁸ Only a monosaccharide unit in heparin fragments H3, H4, and H7 was predicted to make interactions with the GAG binding site, whereas a disaccharide unit present in H5 was predicted to make electrostatic interactions with basic residues in the GAG binding site. Similar docked poses were predicted with the NMR structure.

The predicted measures of binding affinity determined by the AutoDock scoring function were not of the same magnitude as the experimentally determined activity of molecules H5, H6, H7, and H9, although the free energies predicted could differentiate and rank accurately compounds with different degrees of sulfation. Ligand-specific scoring functions such as BALLDock/SLICK^{168,169} and others¹⁷⁰ focused on carbohydrates (simple sugars) have been developed. These scoring functions will need to be calibrated before they can be used for predicting free energies of binding to proteins of sulfated GAGs.

There does not appear to be a simple correlation between the length of the heparin fragments and their free energies of binding in our docking studies, and hence, it was not possible to resolve the controversy regarding the optimum and minimum lengths of the oligosaccharide required for binding to CXCL-8 (vide supra).^{39,58,64} These docking studies suggest that sulfated heparin saccharides with six or less units bind to monomeric CXCL-8 rather than the dimeric structure because heparin fragments

(H1–H12) were seen to bind parallel to the helical axis in the monomers only.

Molecular Docking and Free Energy Calculations of Complexes of Cyclitols with CXCL-8. MD simulations of the CXCL-8 dimer reported above advocated the use of the X-ray structure of the CXCL-8 dimer for docking simulations. Hence, the cyclitols reported in Table 2 were docked to sites 1 and 2 of the CXCL-8 X-ray structure. The interactions of various cyclitols with the CXCL-8 monomer (site 1) predicted by these docking simulations are reported in Table 5. It can be seen that the free energy scores and the binding modes predicted by docking to the CXCL-8 monomer cannot differentiate between the active cyclitols 8, 9, 10, and 10a and other inactive ligands (2–7 and 11–14). For example, cyclitol 3 is predicted to bind with higher affinity to monomeric CXCL-8, in contrast to experimental data that shows that this molecule is incapable of blocking heparin–CXCL-8 interactions.⁷⁶ These results suggest that cyclitols may in fact interact with CXCL-8 through another binding site.

The interactions of cyclitols 2–14 in binding site 2 of dimeric CXCL-8 are reported in Table 5. While the scoring function energies cannot be correlated to earlier-reported SAR studies,⁷⁶ short cyclitols (2–6) are correctly predicted not to bind to CXCL-8. Visualization of the binding modes shows that cyclitols with linker size >7 are able to bridge the two monomers A and B of the CXCL-8 dimer. The hydrophobic linker of size 8 lies perpendicular to the two monomeric chains A and B, and the sulfates make electrostatic interactions with basic residues in the C-terminal α -helices of both monomers, which form the GAG binding site (Figure 10). Similar binding modes were observed for cyclitols 9, 10, and 10a. The sulfates in cyclitols 2–7 and cyclitols 11–12 appear to have a higher number of interactions with the basic residues of one monomer compared to other monomer because the hydrophobic linker in these cyclitols is too short to bridge the two monomers. The sulfonate group (SO_3^-) in cyclitols 13 and 14 might reduce binding due to the presence of a negatively charged region near Glu63. The present docking simulations suggest that not all sulfates on the 6-membered cyclitol ring interact with residues of the CXCL-8 dimer. We were not able to obtain a better binding mode with the NMR structure of the CXCL-8 dimer due to differences in the

Table 5. Docking of Cyclitols to Monomeric and Dimeric CXCL-8

cyclitol no.	AutoDock energy of binding (kcal/mol)	K_i	number of interacting sulfates	interactions between cyclitol sulfates and the sidechains of residues of CXCL-8 within 3.5 Å
docking of cyclitols to CXCL-8 monomer (site 1)				
2	-8.09	1.17 μM	2	Arg60, Lys64
3	-9.94	51 nM	5	Lys20, Lys64, Lys67, Arg68, Asn71
4	-5.39	111.74 μM	4	Lys20, Trp57, Arg60
5	-2.64	11.54 mM	2	Asn56, Lys64
6	-6.45	18.86 μM	3	Lys20, Arg45, Lys64
7	-6.88	9.06 μM	5	His18, Lys67, Lys64, Asn71
8	-6.10	33.76 μM	5	His18, Arg60, Lys64, Lys67, Asn71
9	-4.01	1.14 mM	6	His18, Arg60, Lys64, Lys67, Asn71
10	-4.37	626 μM	4	Lys64, Lys67, Arg68, Asn71
11	-7.57	2.82 mM	3	His18, Arg60, Lys64
12	-5.82	54.30 mM	2	Ser44, Arg47
13	-7.31	4.39 mM	3	His18, Lys20, Lys64
14	-4.09	999.56 mM	3	Phe17, His18, Lys64
6a	-7.14	5.86 μM	3	Lys64, Lys67
10a	-6.67	13.01 μM	6	His18, Lys20, Arg60, Lys64
docking of cyclitols to CXCL-8 dimer (site 2) ^a				
2	+0.28		4	Arg60(A), Lys67(A), Arg60(B)
3	+0.34		3	Lys67(A), Asn56(B), Lys67(B)
4	-0.68	317.86 mM	5	Arg60(A), Lys64(A), Lys67(A), Arg60(B), Lys 67(B)
5	+1.24		3	Arg60(A), Lys64(A), Lys67(A)
6	+0.57		4	Arg60(A), Lys64(A), Lys67(A), Lys67(B)
7	-4.83	286.93 μM	4	Asn56(A), Arg60(A), Lys67(A), Lys67(B)
8	-6.28	24.96 μM	6	Arg60(A), Lys64(A), Lys67(A), Lys67(B), Lys64(B), Arg60(B)
9	-4.86	273.86 μM	5	Lys64(A), Lys67(A), Lys67(B), Arg60(B)
10	-3.67	2.04 mM	4	Lys64(A), Lys67(A), Lys67(B), Arg60(B)
11	-1.71	55.36 mM	4	Arg60(A), Lys64(A), Lys67(A), Lys67(B)
12	-2.18	25.30 mM	3	Asn56(A), Arg60(A), Arg60(B)
13	+0.19		5	Arg60(A), Lys67(A), Asn56(B), Arg60(B),
14	+0.43		5	Arg60(A), Lys67(A), Asn56(B), Lys64(B), Lys67(B)
6a	-4.31	688.34 μM	7	Arg60(A), Lys67(A), Arg60(B), Lys67(B)
10a	+2.87		9	Arg60(A), Lys64(A), Lys67(A), Arg60(B), Lys64(B), Lys67(B)

^a(A) and (B) refer to each monomer of the CXCL-8 dimer.

interhelical distance, the packing interaction between the monomers and the differences in the GAG binding site (*vide supra*).

MM/PB(GB)SA calculations were performed for cyclitols 7, 8, 9, 10, and 10a docked at binding site 2 of the CXCL-8 dimer. The complex of cyclitol 7 and CXCL-8 was taken as reference to establish the SAR between active and inactive molecules. The predicted MM/PB(GB)SA free energy components are reported in Table 6. Cyclitol 7 was observed to drift away from the binding site within 1 ns after removing constraints and then align itself near the C-terminal helix of a single monomer of CXCL-8. The ligand appears to be too short to bridge the two helices of the CXCL-8 dimer. Free energies of binding obtained with the MM/PBSA method can clearly differentiate between cyclitols 8, 9, and 10. Although these free energies of binding cannot be directly compared to experimental inhibition constants, they correctly rank cyclitol 7 as the more active molecule compared to cyclitols 9 and 10. In contrast to experimental data, the complex of cyclitol 10a with CXCL-8 is predicted to have the highest binding affinity. This appears to be due to a higher degree of sulfation, resulting in an increased nonbonded

electrostatic interaction energy. Free energies of binding obtained with the MM/GBSA approach were positive in value for the interaction of cyclitol 10 with the CXCL-8 dimer, due to a positive value of GBELE (Table 6). Exclusive of entropy terms, the GBSA method correctly ranks cyclitol 8 as the most active out of all cyclitols and cyclitol 10 as having a comparable level of inhibition to cyclitol 10a, whereas the PBSA method overestimates the binding affinity of cyclitol 10a, as compared to the experimental data that shows that cyclitol 8 is the most active molecule.

CXCL-8 monomers and dimers exist *in vivo* and their differential binding to CXCR2 and GAGs mediates and regulates *in vivo* neutrophil recruitment.³² However, the CXCL-8 monomer–dimer equilibrium is disturbed in acute or chronic inflammation and tissue injury, which can lead to the increase in dimer concentration and, consequently, to persistent neutrophil infiltration.³² Therefore, in contrast to cyclitols, the design of small molecules that can bind to CXCL-8 dimer interface and consequently impair potential to form dimers will be important for the future rational design of drugs against a wide variety of neutrophil-mediated inflammatory diseases.

Molecular Docking and Molecular Dynamics of the CXCL-8 Dimer in Complex with a 24-mer Heparin Fragment. The 24-mer heparin fragment was divided into two sulfated hexasaccharides consisting of IdoA2S-GlcNS6S residues and two nonsulfated hexasaccharides consisting of GlcNAc-GlcA. The heparin hexasaccharide was initially docked to one of the monomers taken from the

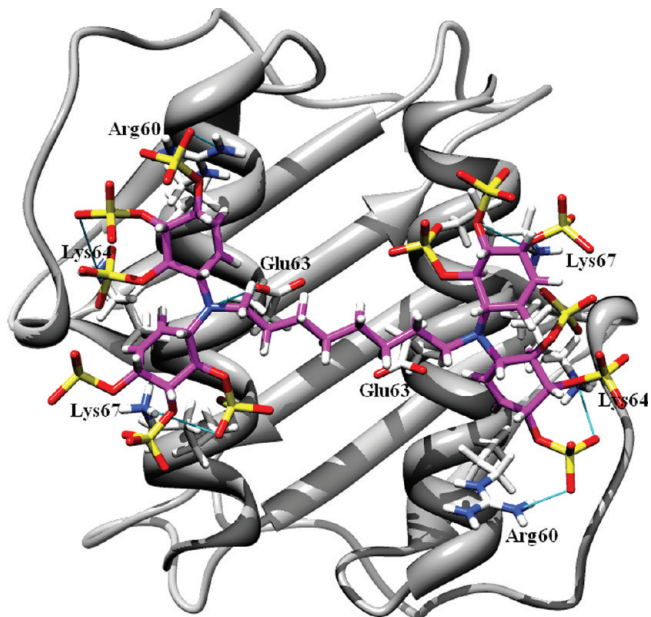


Figure 10. Binding mode and interactions of cyclitol 8 with the CXCL-8 dimer predicted by docking simulations. Interacting residues are represented as sticks. Electrostatic interactions are indicated by blue lines.

structure of the CXCL-8 dimer. Another heparin hexasaccharide was docked into the second, symmetry-related binding site of the other CXCL-8 monomer. The two heparin hexasaccharides were then extended and manually linked with a stretch of two nonsulfated hexasaccharides to form a horseshoe pattern (Figure 11). The interactions of the sulfated heparin fragments with CXCL-8 predicted by docking are reported in Table 7. Most of the interactions of the heparin fragment with CXCL-8 are predicted to be mediated through O-sulfation. It is not meaningful to measure the binding affinity to the CXCL-8 dimer of a 24-mer heparin fragment using the AutoDock scoring function. This scoring function includes a term for the number of rotatable bonds in the ligand (and/or the protein) as an approximation to the entropic cost arising from the loss of conformational degrees of freedom upon binding.¹⁰⁵ However, if the number of rotatable bonds is too large (in this case >60), this term becomes too large, resulting in abnormally large and positive predicted free energies of binding.

MD simulations were then carried out for the complex of the 24-mer heparin fragment with the CXCL-8 dimer. The all-atom rmsd of the protein as well as the sulfated and nonsulfated hexasaccharides were monitored during the simulations (Supporting Information Figure S9A). The nonsulfated fragments were seen to move away from the protein compared to the sulfated fragments, which form direct electrostatic interactions with the protein in this complex. Limited structural change (rmsd of 2.5 Å) was observed within the protein, while the potential energy (Supporting Information Figure S9B), density and temperature of the system were stable during the simulations. On the basis of the measured structural variance and visualization of MD trajectories, an ensemble consisting of at least four sulfated residues in the chair conformation was found to be important for binding to the C-terminal helices of CXCL-8. Our simulations are not consistent with previous MD simulations of this complex where the interaction of CXCL-8 with a single sulfated

Table 6. MM/PB(GB)SA Energy Component Analysis of the Interactions of Cyclitols with the CXCL-8 Dimer Averaged over 8.0 ns^a

	Δ^b CXCL-8-cyclitol 8		Δ^b CXCL-8-cyclitol 9		Δ^b CXCL-8-cyclitol 10		Δ^b CXCL-8-cyclitol 10a	
	mean	std	mean	std	mean	std	mean	std
ELE ^d	-2392.28	88.62	-2496.87	99.64	-3087.14	73.98	-4951.51	102.78
VDW ^e	-28.75	5.4	-38.73	4.33	-32.88	6.53	-22.56	5.93
INT ^f	0	0	0	0	0	0	0	0
GAS ^g	-2421.04	87.82	-2535.59	100.5	-3120.02	75.97	-4974.07	103.6
PBSUR ^h	-5.68	0.3	-6.52	0.22	-5.99	0.5	-5.43	0.4
PBCAL ⁱ	2331.11	78.9	2455.45	90.46	3039.81	72.39	4858.06	96.3
PBSOL ^j	2325.43	78.17	2448.93	90.41	3033.82	72.09	4852.63	96.16
PBELE ^k	-61.17	16.78	-41.42	17.14	-47.33	15.69	-93.45	17.53
PBTOT ^l	-95.6	15.45	-86.67	17.04	-86.2	12.75	-121.44	16.23
GBSUR ^m	-5.68	0.3	-6.52	0.22	-5.99	0.5	-5.43	0.4
GBCAL ⁿ	2374.28	81.44	2494.62	93.97	3091.32	73.08	4945.81	99.5
GBSOL ^o	2368.6	81.43	2488.1	93.92	3085.32	72.79	4940.38	99.35
GBELE ^p	-18	11.74	-2.25	9.55	4.17	12.11	-5.7	13.57
GBTOT ^q	-52.43	10.72	-47.5	9.51	-34.7	8.81	-33.68	11.57
T Δ S ^r	-41.09		-42.16		-40.10		-46.84	
$\Delta G_{\text{binding-PBSA}}^s$	-54.51		-44.51		-46.1		-74.6	
$\Delta G_{\text{binding-GBSA}}^s$	-11.34		-5.34		+5.4		-13.16	

^a Average over 800 snapshots of the MD simulation trajectory. ^b Δ is the average free energy of binding. ^c Entropy calculations were based on normal modes analysis using 40 snapshots. ^d Nonbonded electrostatic energy. ^e Nonbonded van der Waals energy. ^f Bond, angle, dihedral energies. ^g ELE + VDW + INT. ^h Hydrophobic contribution to solvation free energy for PB calculations. ⁱ Reaction field energy calculated by PB. ^j PBSUR + PBCAL. ^k PBCAL + ELE. ^l PBSOL + GAS. ^m Hydrophobic contributions to solvation free energy for GB calculations. ⁿ Reaction field energy calculated by GB. ^o GBSUR + GBCAL. ^p GBCAL + ELE. ^q GBSOL + GAS. ^r T = temperature, ΔS = sum of rotational, translational, and vibrational entropies. ^s Total free energy of binding.

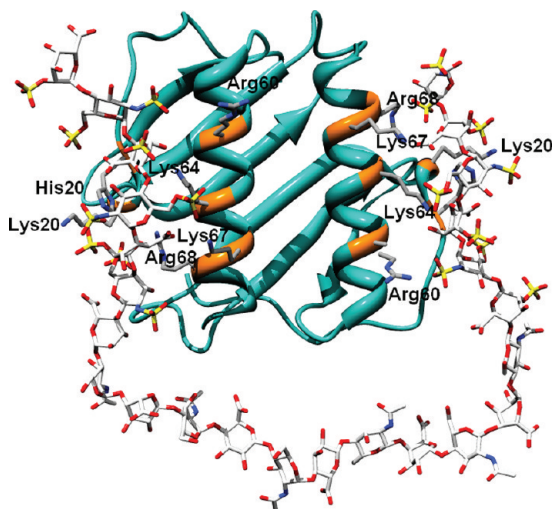


Figure 11. Interactions of the 24-mer heparin fragment with the CXCL-8 dimer. Interacting residues are represented as sticks. Only basic amino acids within 3.5 Å of the fragment are shown.

Table 7. Interactions of the Sulfated Domain of a 24-mer Heparin Fragment with the CXCL-8 Dimer

residues of the sulfated saccharides	interaction with residues of CXCL-8
IdoA2S (COO^-)	sidechain of Lys64
IdoA2S (2-O-sulfate)	sidechain of Lys20, sidechain of Lys64
GlcNS6S (6-O-sulfate)	sidechain of Arg68, backbone of His18, sidechain of Lys64
GlcNS6S (N-sulfate)	

disaccharide unit from the 24-mer fragment had been retained at the end of a 5.0 ns simulation.⁶⁴ In our study, the sulfated heparin fragments retain the electrostatic interactions with the proximal loop and C-terminal helices over 50.0 ns of simulation time. This discrepancy may be due to differences in docking approaches, as the selection of a badly docked conformation of a long heparin fragment may result in the ligand moving away from the binding site during an MD simulation. On the other hand, our simulations do agree with the observation that a single disaccharide unit with 2- and 6-sulfate groups is sufficient to achieve high affinity of binding to CXCL-8 in a multivalent model, as shown in Figure 9D. The low value of the free energy of binding predicted using the MM/PB(GB)SA method (Supporting Information Table S3) suggests that the most important energy contributions come from the interactions of various monosaccharide units present in the 24-mer fragment with CXCL-8 during the simulation, rather than just the interaction of a single disaccharide unit with the CXCL-8 dimer.

The predicted free energies of binding of CXCL-8 with cyclitols, a receptor fragment, and a 24-mer heparin fragment, as documented in Tables 5, S2 and S3 (of the Supporting Information), respectively, cannot be compared quantitatively with experimentally obtained K_d values. This can be attributed to the approximations involved in the MM/PB(GB)SA method and, more importantly, to the lack of reparameterization in the current PB or GB methods to deal with the desolvation and entropic terms of highly charged sulfated carbohydrates such as GAGs.^{166,167} Moreover, inaccurate representation of the in-

ternal dynamics of carbohydrates, is likely to lead to insufficient sampling of glycosidic linkage and ring conformations that contribute to the free energy of binding.¹⁷¹ A further approximation arises from the choice of treatment of 1–4 nonbonded interactions in force fields during MD simulations of glycoproteins.¹⁷² While default 1–4 scaling may be appropriate for the protein, this may be inaccurate for the treatment of nonbonded interactions in carbohydrate force fields, which would affect the accuracy of predictions of free energies. In the context of proteins, the significant difference in free energies of binding with respect to the experimental values may arise due to an incorrect balance of enthalpic and entropic contributions in simulations using the AMBER ff99SB force field.¹⁷³ In addition, estimates of the free energy, enthalpy, and entropy are also dependent on the choice of water potential.¹⁷⁴

CONCLUSIONS

In this paper, various studies of CXCL-8 performed using sequence, structure, and molecular dynamics methods are reported. Evolutionary sequence conservation analysis showed that the GAG binding site is highly variable, suggesting that CXCL-8 across different species may bind GAGs with different sulfation patterns and with different affinity. Residues in the third β -sheet of CXCL-8 were found to be highly variable, while the second β -sheet appears highly conserved. Residues in the first β -sheet, which forms the dimer interface, appear to be partially conserved, based on an analysis of the CXCL-8 monomer. A survey of sulfate-binding regions in the PDB database revealed several occurrences of positively charged regions on the protein surface which form the binding site for sulfated GAGs such as heparin/HS, in agreement with the GAG binding site reported on the basis of analysis of mutagenesis data.

The interaction of CXCL-8 and its receptor CXCR-1 was examined using the experimental structure of CXCL-8 bound to a synthetic 17-amino acid peptide derived from CXCR1. A large degree of structural disorder for residues Met1–Met8 of CXCR1 was observed during MD simulations, indicating that this part of the peptide is bound loosely to CXCL-8. Our simulations suggest that, apart from hydrophobic interactions, aromatic and electrostatic interactions also play a role in mediating contacts between CXCL-8 and the synthetic receptor peptide and that it may be worth re-examining the role of these interactions experimentally. These findings may help to identify peptides derived from one of the protein binding partners with enhanced affinity and serve as starting point for the development of protein–protein inhibitors. Such molecules may have a role in inflammation by inhibiting the superfluous association of neutrophils to the endothelial cell surface, thus reducing damage to host tissue.

MD simulations of the NMR structure of the CXCL-8 dimer revealed that the interhelical distance approaches the interhelical distance observed in the X-ray structure, suggesting that the latter is a better representation of the structure of the dimer, which can be used for designing ligands such as cyclitols. The simulations also showed changes in the secondary structures of the N-terminal loop, the 3₁₀-helix, the 30s, 40s, and 50s loops, and the third β -sheet of CXCL-8 in a concerted manner, accompanying the shearing movements of these C-terminal helices in the CXCL-8 dimer.

Molecular docking of heparin fragments showed low energy docking poses of sulfated heparin being clustered in locations parallel to the C-terminal helical axis of the X-ray structure of

CXCL-8. Docking of disaccharide fragments resulted in many docking pose clusters around basic residues, suggesting that they can bind either the CXCL-8 monomer or dimer in multivalent mode. The docking simulations also suggested that most of the interactions of heparin fragments with the GAG binding site of CXCL-8 are mediated through O-sulfate groups. It is proposed that sulfated heparin saccharide fragments (with six or fewer sugar units) bind to monomeric CXCL-8, whereas longer heparin fragments can bridge the two dimers. The binding of cyclitols to CXCL-8 requires a dimer, and this binding pattern appears to be analogous to the proposed horseshoe binding pattern of a 24-mer heparin fragment. Our simulations provide a rationale for the optimal number of sulfates and the length of alkyl spacers required for the interaction of this type of inhibitors with the dimeric form of CXCL-8. In summary, these modeling studies suggest a possible avenue for therapeutic applications as they predict that the conformational changes of dimeric CXCL-8 may be relevant for the rational design of CXCL-8 inhibitors (carbohydrate or peptide based).

■ ASSOCIATED CONTENT

Supporting Information. Accession numbers for CXCL-8 from various species and percentage identity with respect to human CXCL-8 (Table S1), MM/PB(GB)SA energy component analysis of the interactions of the CXCL-8 dimer with the receptor peptide averaged over 50 ns (Table S2), MM/PB(GB)SA energy component analysis of the interactions of the CXCL-8 dimer with a 24-mer heparin fragment averaged over 50 ns (Table S3), chemical structure of the 24-mer heparin fragment (Figure S1), amino acid residue conservation in the structure of CXCL-8 (PDB code: 3IL8) obtained using default Consurf parameters (Figure S2), multiple sequence alignment of CXCL-8 homologous sequences obtained using Consurf DB (Figure S3), multiple sequence alignment of CXCL-8 protein sequences collected from SWISS-PROT using a BLAST search as mentioned in Table S1 (Figure S4), ribbon diagrams highlighting those residues in the CXCL-8 dimer (taken from the X-ray structure, PDB code: 3IL8) involved in the binding to receptors and GAGs (Figure S5), time evolution of the average backbone rmsd of the whole CXCL-8 dimer, the two C-terminal helices of CXCL-8 and the receptor peptide (Figure S6), secondary structure “dynamic conservation” analysis using the DSSP method in the simulation starting from the NMR structure (Figure S7), secondary structure dynamic conservation analysis using the DSSP method in the simulation starting from the X-ray structure (Figure S8), time evolution of the average all-atom RMSD of the CXCL-8 dimer, the two sulfated and two non-sulfated regions of the 24-mer heparin fragment. The non-sulfated region of heparin is more flexible compared to the sulfated regions, which are bound to the protein in the CXCL-8-heparin complex (Figure S9). The output of normal modes calculations in PDB format corresponding to the sixteenth and eighteenth lowest frequency modes are provided as ci1003366_si_002.pdb and ci1003366_si_003.pdb. The Consurf and MM/PB(GB)SA methods are also described in detail. This information is available free of charge via the Internet at <http://pubs.acs.org>.

■ AUTHOR INFORMATION

Corresponding Author

*E-mail: r.mancera@curtin.edu.au. Phone: +61 8 9266 1017.
Fax: +61 8 9266 2342.

■ ACKNOWLEDGMENT

N.S.G. is grateful for the award of an Endeavour International Postgraduate Research Studentship. We also gratefully acknowledge the Western Australian Interactive Virtual Environments Centre (IVEC) and the National Computational Infrastructure (NCI) Facility for access to high-performance computing.

■ REFERENCES

- Iizasa, H.; Matsushima, K., IL-8. In *Cytokine reference: a compendium of cytokines and other mediators of host defense*; Oppenheim, J. J., Feldmann, M., Durum, S. K., Hirano, T., Vilcek, J., Nicola, N. A., Eds.; Academic Press: New York, 2001; Vol. I, pp 1061–1068.
- Bagliolini, M.; Clark-Lewis, I. Interleukin-8, a chemotactic and inflammatory cytokine. *FEBS Lett.* **1992**, *307*, 97–101.
- Murphy, P. Neutrophil receptors for interleukin-8 and related CXC chemokines. *Semin. Hematol.* **1997**, *34*, 311–318.
- Hoch, R. C.; Schraufstatter, I. U.; Cochrane, C. G. In vivo, in vitro, and molecular aspects of interleukin-8 and the interleukin-8 receptors. *J. Lab. Clin. Med.* **1996**, *128*, 134–145.
- Bagliolini, M.; Walz, A.; Kunkel, S. L. Neutrophil-activating peptide-1/interleukin 8, a novel cytokine that activates neutrophils. *J. Clin. Invest.* **1989**, *84*, 1045–1049.
- Norgauer, J.; Krutmann, J.; Dobos, G. J.; Traynor-Kaplan, A. E.; Oades, Z. G.; Schraufstatter, I. U. Actin polymerization, calcium-transients, and phospholipid metabolism in human neutrophils after stimulation with interleukin-8 and N-formyl peptide. *J. Invest. Dermatol.* **1994**, *102*, 310–314.
- Middleton, J.; Patterson, A. M.; Gardner, L.; Schmutz, C.; Ashton, B. A. Leukocyte extravasation: chemokine transport and presentation by the endothelium. *Blood* **2002**, *100*, 3853–3860.
- Sekido, N.; Mukaida, N.; Harada, A.; Nakanishi, I.; Watanabe, Y.; Matsushima, K. Prevention of lung reperfusion injury in rabbits by a monoclonal antibody against interleukin-8. *Nature* **1993**, *365*, 654–657.
- Bizzarri, C.; Allegretti, M.; Bitondo, R. D.; Cervellera, M. N.; Colotta, F.; Bertini, R. Pharmacological inhibition of interleukin-8 (CXCL8) as a new approach for the prevention and treatment of several human diseases. *Curr. Med. Chem. Anti-Inflamm. Anti. Allergy Agents* **2003**, *2*, 67–79.
- Duan, H.; Koga, T.; Kohda, F.; Hara, H.; Urabe, K.; Furue, M. Interleukin-8-positive neutrophils in psoriasis. *J. Dermatol. Sci.* **2001**, *26*, 119–124.
- Chollet-Martin, S.; Montravers, P.; Gibert, C.; Elbim, C.; Desmonts, J. M.; Fagon, J. Y.; Gougerot-Pocidalo, M. A. High levels of interleukin-8 in the blood and alveolar spaces of patients with pneumonia and adult respiratory distress syndrome. *Infect. Immun.* **1993**, *61*, 4553–4559.
- Carré, P. C.; Mortenson, R. L.; King, T. E.; Noble, P. W.; Sable, C. L.; Riches, D. W. Increased expression of the interleukin-8 gene by alveolar macrophages in idiopathic pulmonary fibrosis. A potential mechanism for the recruitment and activation of neutrophils in lung fibrosis. *J. Clin. Invest.* **1991**, *88*, 1802–1810.
- Miller, E. J.; Cohen, A. B.; Nagao, S.; Griffith, D.; Maunder, R. J.; Martin, T. R.; Weiner-Kronish, J. P.; Sticherling, M.; Christophers, E.; Matthay, M. A. Elevated levels of NAP-1/interleukin-8 are present in the airspaces of patients with the adult respiratory distress syndrome and are associated with increased mortality. *Am. Rev. Respir. Dis.* **1992**, *146*, 427–432.
- Lynch, J. P., 3rd; Standiford, T. J.; Rolfe, M. W.; Kunkel, S. L.; Strieter, R. M. Neutrophilic alveolitis in idiopathic pulmonary fibrosis. The role of interleukin-8. *Am. Rev. Respir. Dis.* **1992**, *145*, 1433–1439.
- Strieter, R. M.; Polverini, P. J.; Arenberg, D. A.; Walz, A.; Opdenakker, G.; Vandamme, J.; Kunkel, S. L. Role of C-X-C chemokines as regulators of angiogenesis in lung-cancer. *J. Leukoc. Biol.* **1995**, *57*, 752–762.
- Koch, A. E.; Polverini, P. J.; Kunkel, S. L.; Harlow, L. A.; Dipietro, L. A.; Elner, V. M.; Elner, S. G.; Strieter, R. M. Interleukin-8 as a macrophage-derived mediator of angiogenesis. *Science* **1992**, *258*, 1798–1801.

- (17) Zlotnik, A.; Yoshie, O. Chemokines: A new classification system and their role in immunity. *Immunity* **2000**, *12*, 121–127.
- (18) Baggolini, M.; Dewald, B.; Moser, B. Interleukin-8 and related chemotactic cytokines—CXC and CC chemokines. *Adv. Immunol.* **1994**, *55*, 97–179.
- (19) Fernandez, E. J.; Lolis, E. Structure, function, and inhibition of chemokines. *Annu. Rev. Pharmacol. Toxicol.* **2002**, *42*, 469–499.
- (20) Rajarathnam, K.; Sykes, B. D.; Dewald, B.; Baggolini, M.; Clark-Lewis, I. Disulfide bridges in interleukin-8 probed using non-natural disulfide analogues: Dissociation of roles in structure from function. *Biochemistry* **1999**, *38*, 7653–7658.
- (21) Clark-Lewis, I.; Dewald, B.; Loetscher, M.; Moser, B.; Baggolini, M. Structural requirements for interleukin-8 function identified by design of analogs and CXC chemokine hybrids. *J. Biol. Chem.* **1994**, *269*, 16075–16081.
- (22) Webb, L. M.; Ehrengruber, M. U.; Clark-Lewis, I.; Baggolini, M.; Rot, A. Binding to heparan sulfate or heparin enhances neutrophil responses to interleukin 8. *Proc. Natl. Acad. Sci. U.S.A.* **1993**, *90*, 7158–7162.
- (23) Hammond, M. E.; Shyamala, V.; Siani, M. A.; Gallegos, C. A.; Feucht, P. H.; Abbott, J.; Lapointe, G. R.; Moghadam, M.; Khoja, H.; Zakel, J. Receptor recognition and specificity of interleukin-8 is determined by residues that cluster near a surface-accessible hydrophobic pocket. *J. Biol. Chem.* **1996**, *271*, 8228–8235.
- (24) David, R.; Günther, R.; Baumann, L.; Lühmann, T.; Seebach, D.; Hofmann, H.-J. r.; Beck-Sickinger, A. G. Artificial chemokines: Combining chemistry and molecular biology for the elucidation of interleukin-8 functionality. *J. Am. Chem. Soc.* **2008**, *130*, 15311–15317.
- (25) Skelton, N. J.; Quan, C.; Reilly, D.; Lowman, H. Structure of a CXC chemokine-receptor fragment in complex with interleukin-8. *Structure* **1999**, *7*, 157–168.
- (26) Clore, G. M.; Appella, E.; Yamada, M.; Matsushima, K.; Gronenborn, A. M. Three-dimensional structure of interleukin 8 in solution. *Biochemistry* **1990**, *29*, 1689–1696.
- (27) Rajarathnam, K.; Clark-Lewis, I.; Sykes, B. D. ¹H NMR solution structure of an active monomeric interleukin-8. *Biochemistry* **1995**, *34*, 12983–12990.
- (28) Baldwin, E. T.; Weber, I. T.; St Charles, R.; Xuan, J. C.; Appella, E.; Yamada, M.; Matsushima, K.; Edwards, B. F.; Clore, G. M.; Gronenborn, A. M. Crystal structure of interleukin 8: symbiosis of NMR and crystallography. *Proc. Natl. Acad. Sci. U.S.A.* **1991**, *88*, 502–506.
- (29) Baldwin, E. T.; Franklin, K. A.; Appella, E.; Yamada, M.; Matsushima, K.; Wlodawer, A.; Weber, I. T. Crystallization of human interleukin-8. A protein chemotactic for neutrophils and T-lymphocytes. *J. Biol. Chem.* **1990**, *265*, 6851–6853.
- (30) Gerber, N.; Lowman, H.; Artis, D. R.; Eigenbrot, C. Receptor-binding conformation of the “ELR” motif of IL-8: X-ray structure of the L5C/H33C variant at 2.35 Å resolution. *Proteins* **2000**, *38*, 361–367.
- (31) Eigenbrot, C.; Lowman, H. B.; Chee, L.; Artis, D. R. Structural change and receptor binding in a chemokine mutant with a rearranged disulfide: X-ray structure of e38C/C50A IL-8 at 2 Å resolution. *Proteins* **1997**, *27*, 556–566.
- (32) Das, S. T.; Rajagopalan, L.; Guerrero-Plata, A.; Sai, J.; Richmond, A.; Garofalo, R. P.; Rajarathnam, K. Monomeric and dimeric CXCL8 are both essential for in vivo neutrophil recruitment. *PLoS ONE* **2010**, *5*, e11754.
- (33) Leong, S. R.; Lowman, H. B.; Liu, J.; Shire, S.; Deforge, L. E. Gillece-Castro, B. L.; McDowell, R.; Hebert, C. A. IL-8 single-chain homodimers and heterodimers: interactions with chemokine receptors CXCR1, CXCR2, and DARC. *Protein Sci.* **1997**, *6*, 609–617.
- (34) Rajarathnam, K.; Kay, C. M.; Clark-Lewis, I. Sykes, B. D. Characterization of quaternary structure of interleukin-8 and functional implications. *Methods Enzymol.* **1997**, *287*, 89–105.
- (35) Lowman, H. B.; Fairbrother, W. J.; Slagle, P. H.; Kabakoff, R. Liu, J.; Shire, S.; Hebert, C. A. Monomeric variants of IL-8: Effects of side chain substitutions and solution conditions upon dimer formation. *Protein Sci.* **1997**, *6*, 598–608.
- (36) Burrows, S. D.; Doyle, M. L.; Murphy, K. P.; Franklin, S. G.; White, J. R.; Brooks, I.; McNulty, D. E.; Scott, M. O.; Knutson, J. R. Determination of the monomer-dimer equilibrium of interleukin-8 reveals it is a monomer at physiological concentrations. *Biochemistry* **1994**, *33*, 12741–12745.
- (37) Paolini, J. F.; Willard, D.; Consler, T.; Luther, M.; Krangell, M. S. The chemokines IL-8, monocyte chemoattractant protein-1, and I-309 are monomers at physiologically relevant concentrations. *J. Immunol.* **1994**, *153*, 2704–2717.
- (38) Henry, B. L.; Wayne, J. F.; Paul, H. S.; Rhona, K.; Caroline, A. H.; Jun, L.; Steven, S. Monomeric variants of IL-8: Effects of side chain substitutions and solution conditions upon dimer formation. *Protein Sci.* **1997**, *6*, 598–608.
- (39) Goger, B.; Halden, Y.; Rek, A.; Mosl, R.; Pye, D.; Gallagher, J.; Kungl, A. J. Different affinities of glycosaminoglycan oligosaccharides for monomeric and dimeric interleukin-8: A model for chemokine regulation at inflammatory sites. *Biochemistry* **2002**, *41*, 1640–1646.
- (40) Nesmelova, I. V.; Sham, Y.; Dudek, A. Z.; van Eijk, L. I.; Wu, G.; Slungaard, A.; Mortari, F.; Griffioen, A. W.; Mayo, K. H. Platelet factor 4 and interleukin-8 CXC chemokine heterodimer formation modulates function at the quaternary structural level. *J. Biol. Chem.* **2005**, *280*, 4948–4958.
- (41) Cornell, W.; Abseher, R.; Nilges, M.; Case, D. A. Continuum solvent molecular dynamics study of flexibility in interleukin-8. *J. Mol. Graph. Model.* **2001**, *19*, 136–145.
- (42) Chunthrapai, A.; Kim, K. J. Regulation of the expression of IL-8 receptor A/B by IL-8: possible functions of each receptor. *J. Immunol.* **1995**, *155*, 2587–2594.
- (43) Lee, J.; Horuk, R.; Rice, G. C.; Bennett, G. L.; Camerato, T.; Wood, W. I. Characterization of two high affinity human interleukin-8 receptors. *J. Biol. Chem.* **1992**, *267*, 16283–16287.
- (44) Murphy, P. M.; Tiffany, H. L. Cloning of complementary DNA encoding a functional human interleukin-8 receptor. *Science* **1991**, *253*, 1280–1283.
- (45) Holmes, W. E.; Lee, J.; Kuang, W. J.; Rice, G. C.; Wood, W. I. Structure and functional expression of a human interleukin-8 receptor. *Science* **1991**, *253*, 1278–1280.
- (46) Ahuja, S. K.; Murphy, P. M. The CXC chemokines growth-regulated oncogene (GRO) alpha, GRObeta, GROgamma, neutrophil-activating peptide-2, and epithelial cell-derived neutrophil-activating peptide-78 are potent agonists for the type B, but not the type A, human interleukin-8 receptor. *J. Biol. Chem.* **1996**, *271*, 20545–20550.
- (47) Zhao-hai, L.; Zi-xuan, W.; Horuk, R.; Hesselgesser, J.; Yan-chun, L.; Hadley, T. J.; Peiper, S. C. The promiscuous chemokine binding profile of the duffy antigen/receptor for chemokines is primarily localized to sequences in the amino-terminal domain. *J. Biol. Chem.* **1995**, *270*, 26239–26245.
- (48) Hébert, C. A.; Vitangcol, R. V.; Baker, J. B. Scanning mutagenesis of interleukin-8 identifies a cluster of residues required for receptor binding. *J. Biol. Chem.* **1991**, *266*, 18989–18994.
- (49) LaRosa, G. J.; Thomas, K. M.; Kaufmann, M. E.; Mark, R.; White, M.; Taylor, L.; Gray, G.; Witt, D.; Navarro, J. Amino terminus of the interleukin-8 receptor is a major determinant of receptor subtype specificity. *J. Biol. Chem.* **1992**, *267*, 25402–25406.
- (50) Rajagopalan, L.; Rajarathnam, K. Ligand selectivity and affinity of chemokine receptor CXCR1: Role of N-terminal domain. *J. Biol. Chem.* **2004**, *279*, 30000–30008.
- (51) Gayle, R. B. d.; Sleath, P. R.; Srinivasan, S.; Birks, C. W.; Weerawarna, K. S.; Cerretti, D. P.; Kozlosky, C. J.; Nelson, N.; Vandenberg Bos, T.; Beckmann, M. P. Importance of the amino terminus of the interleukin-8 receptor in ligand interactions. *J. Biol. Chem.* **1993**, *268*, 7283–7289.
- (52) Attwood, M. R.; Conway, E. A.; Dunsdon, R. M.; Greening, J. R.; Handa, B. K.; Jones, P. S.; Jordan, S. C.; Keech, E.; Wilson, F. X. Peptide based inhibitors of interleukin-8: structural simplification and enhanced potency. *Bioorg. Med. Chem. Lett.* **1997**, *7*, 429–432.
- (53) Leong, S. R.; Kabakoff, R. C.; Hebert, C. A. Complete mutagenesis of the extracellular domain of interleukin-8 (IL-8) type A receptor identifies charged residues mediating IL-8 binding and signal transduction. *J. Biol. Chem.* **1994**, *269*, 19343–19348.
- (54) Clubb, R. T.; Omichinski, J. G.; Clore, G. M.; Gronenborn, A. M. Mapping the binding surface of interleukin-8 complexed with an

- N-terminal fragment of the Type 1 human interleukin-8 receptor. *FEBS Lett.* **1994**, *338*, 93–97.
- (55) Ravindran, A.; Joseph, P. R. B.; Rajarathnam, K. Structural basis for differential binding of the Interleukin-8 monomer and dimer to the CXCR1 N-Domain: Role of coupled interactions and dynamics. *Biochemistry* **2009**, *48*, 8795–8805.
- (56) Luo, Z.; Butcher, D. J.; Huang, Z. Molecular modeling of interleukin-8 receptor beta and analysis of the receptor-ligand interaction. *Protein Eng.* **1997**, *10*, 1039–1045.
- (57) Kuschert, G. S.; Hoogewerf, A. J.; Proudfoot, A. E.; Chung, C. W.; Cooke, R. M.; Hubbard, R. E.; Wells, T. N.; Sanderson, P. N. Identification of a glycosaminoglycan binding surface on human interleukin-8. *Biochemistry* **1998**, *37*, 11193–11201.
- (58) Kuschert, G. S.; Coulin, F.; Power, C. A.; Proudfoot, A. E.; Hubbard, R. E.; Hoogewerf, A. J.; Wells, T. N. Glycosaminoglycans interact selectively with chemokines and modulate receptor binding and cellular responses. *Biochemistry* **1999**, *38*, 12959–12968.
- (59) Spillmann, D.; Witt, D.; Lindahl, U. Defining the interleukin-8-binding domain of heparan sulfate. *J. Biol. Chem.* **1998**, *273*, 15487–15493.
- (60) Steven, R. L.; Caroline, A. H.; Henry, B. L.; Jun, L.; Steven, S.; Laura, E. D.; Beth, L. G.-C.; Robert, M. IL-8 single-chain homodimers and heterodimers: Interactions with the chemokine receptors CXCR1, CXCR2, and DARC. *Protein Sci.* **1997**, *6*, 609–617.
- (61) Rajarathnam, K.; Prado, G. N.; Fernando, H.; Clark-Lewis, I.; Navarro, J. Probing receptor binding activity of interleukin-8 dimer using a disulfide trap. *Biochemistry* **2006**, *45*, 7882–7888.
- (62) Fernando, H.; Chin, C.; Rosgen, J.; Rajarathnam, K. Dimer dissociation is essential for interleukin-8 (IL-8) binding to CXCR1 receptor. *J. Biol. Chem.* **2004**, *279*, 36175–36178.
- (63) Rajarathnam, K.; Sykes, B. D.; Kay, C. M.; Dewald, B.; Geiser, T.; Baggolini, M.; Clark-Lewis, I. Neutrophil activation by monomeric interleukin-8. *Science* **1994**, *264*, 90–92.
- (64) Krieger, E.; Geretti, E.; Brandner, B.; Goger, B.; Wells, T. N.; Kungl, A. J. A structural and dynamic model for the interaction of interleukin-8 and glycosaminoglycans: support from isothermal fluorescence titrations. *Proteins* **2004**, *54*, 768–775.
- (65) Lortat-Jacob, H.; Grosdidier, A.; Imbert, A. Structural diversity of heparan sulfate binding domains in chemokines. *Proc. Natl. Acad. Sci. U.S.A.* **2002**, *99*, 1229–1234.
- (66) Bitomsky, W.; Wade, R. C. Docking of glycosaminoglycans to heparin-binding proteins: validation for aFGF, bFGF, and antithrombin and application to IL-8. *J. Am. Chem. Soc.* **1999**, *121*, 3004–3013.
- (67) de Paz, J. L.; Moseman, E. A.; Noti, C.; Polito, L.; von Andrian, U. H.; Seeberger, P. H. Profiling heparin-chemokine interactions using synthetic tools. *ACS Chem. Biol.* **2007**, *2*, 735–744.
- (68) Hay, D. W. P.; Sarau, H. M. Interleukin-8 receptor antagonists in pulmonary diseases. *Curr. Opin. Pharmacol.* **2001**, *1*, 242–247.
- (69) Li, F.; Gordon, J. R. IL-8(3–73)K11R is a high affinity agonist of the neutrophil CXCR1 and CXCR2. *Biochem. Biophys. Res. Commun.* **2001**, *286*, 595–600.
- (70) Moser, B.; Dewald, B.; Barella, L.; Schumacher, C.; Baggolini, M.; Clark-Lewis, I. Interleukin-8 antagonists generated by N-terminal modification. *J. Biol. Chem.* **1993**, *268*, 7125–7128.
- (71) Li, F.; Zhang, X.; Gordon, J. R. CXCL8(3–73)K11R/G31P antagonizes ligand binding to the neutrophil CXCR1 and CXCR2 receptors and cellular responses to CXCL8/IL-8. *Biochem. Biophys. Res. Commun.* **2002**, *293*, 939–944.
- (72) Attwood, M. R.; Borkakoti, N.; Bottomley, G. A.; Conway, E. A.; Cowan, I.; Fallowfield, A. G.; Handa, B. K.; Jones, P. S.; Keech, E.; Kirtland, S. J.; Williams, G.; Wilson, F. X. Identification and characterisation of an inhibitor of interleukin-8: a receptor based approach. *Bioorg. Med. Chem. Lett.* **1996**, *6*, 1869–1874.
- (73) Busch-Petersen, J. Small molecule antagonists of the CXCR2 and CXCR1 chemokine receptors as therapeutic agents for the treatment of inflammatory diseases. *Curr. Top. Med. Chem.* **2006**, *6*, 1345–1352.
- (74) Bedke, J.; Nelson, P. J.; Kiss, E.; Muenchmeier, N.; Rek, A.; Behnes, C.-L.; Gretz, N.; Kungl, A. J.; Gröne, H.-J. A novel CXCL8 protein-based antagonist in acute experimental renal allograft damage. *Mol. Immunol.* **2010**, *47*, 1047–1057.
- (75) Rek, A.; Potzinger, H.; Wabitsch, V.; Geretti, E.; Piccinini, M. A.; Falsone, S. F.; Grosse Kracht, S.; Teixeira, M.; Adage, T.; Kungl, A. J. Turning the glycan switch to change CXCL8 into a potent anti-inflammatory biological drug. *Proc. Natl. Acad. Sci. U.S.A.* **2010**, submitted for publication.
- (76) Freeman, C.; Liu, L.; Banwell, M. G.; Brown, K. J.; Bezios, A.; Ferro, V.; Parish, C. R. Use of sulfated linked cyclitols as heparan sulfate mimetics to probe the heparin/heparan sulfate binding specificity of proteins. *J. Biol. Chem.* **2005**, *280*, 8842–8849.
- (77) Altschul, S. F.; Madden, T. L.; Schaffer, A. A.; Zhang, J.; Zhang, Z.; Miller, W.; Lipman, D. J. Gapped BLAST and PSI-BLAST: a new generation of protein database search programs. *Nucleic Acids Res.* **1997**, *25*, 3389–3402.
- (78) Boeckmann, B.; Bairoch, A.; Apweiler, R.; Blatter, M.-C.; Estreicher, A.; Gasteiger, E.; Martin, M. J.; Michoud, K.; O'Donovan, C.; Phan, I.; Pilbaut, S.; Schneider, M. The SWISS-PROT protein knowledgebase and its supplement TrEMBL in 2003. *Nucleic Acids Res.* **2003**, *31*, 365–370.
- (79) Landau, M.; Mayrose, I.; Rosenberg, Y.; Glaser, F.; Martz, E.; Pupko, T.; Ben-Tal, N. ConSurf 2005: the projection of evolutionary conservation scores of residues on protein structures. *Nucleic Acids Res.* **2005**, *33*, W299–W302.
- (80) Rambaut, A. *FigTree, a graphical viewer of phylogenetic trees*, 1.2.2; Institute of Evolutionary Biology: Edinburgh, 2006.
- (81) Suhre, K.; Sanejouand, Y.-H. EINemo: a normal mode web server for protein movement analysis and the generation of templates for molecular replacement. *Nucleic Acids Res.* **2004**, *32*, W610–W614.
- (82) Maple, J. R. Derivation of class II force fields: V. Quantum force field for amides, peptides, and related compounds. *J. Comput. Chem.* **1998**, *19*, 430–458.
- (83) Dealwis, C.; Fernandez, E. J.; Thompson, D. A.; Simon, R. J.; Siani, M. A.; Lolis, E. Crystal structure of chemically synthesized [N33A] stromal cell-derived factor 1 α , a potent ligand for the HIV-1 “fusin” coreceptor. *Proc. Natl. Acad. Sci. U.S.A.* **1998**, *95*, 6941–6946.
- (84) Lubkowski, J.; Bujacz, G.; Boqué, L.; Domaille, P. J.; Handel, T. M.; Alexander, W. The structure of MCP-1 in two crystal forms provides a rare example of variable quaternary interactions. *Nat. Struct. Biol.* **1997**, *4*, 64–69.
- (85) Hoover, D. M.; Shaw, J.; Gryczynski, Z.; Proudfoot, A. E. I.; Wells, T.; Lubkowski, J. The crystal structure of Met-Rantes: comparison with native Rantes and AOP-Rantes. *Protein Pept. Lett.* **2000**, *7*, 73–82.
- (86) Gandhi, N. S.; Coombe, D. R.; Mancera, R. L. Platelet endothelial cell adhesion molecule 1 (PECAM-1) and its interactions with glycosaminoglycans: I. Molecular modeling studies. *Biochemistry* **2008**, *47*, 4851–4862.
- (87) Krissinel, E.; Henrick, K. Secondary-structure matching (SSM), a new tool for fast protein structure alignment in three dimensions. *Acta Cryst. Sect. D* **2004**, *60*, 2256–2268.
- (88) Krissinel, E.; Henrick, K. Protein structure comparison service SSM at European Bioinformatics Institute. <http://www.ebi.ac.uk/msd-srv/ssm> (November 15).
- (89) Showalter, S. A.; Brüschweiler, R. Quantitative molecular ensemble interpretation of NMR dipolar couplings without restraints. *J. Am. Chem. Soc.* **2007**, *129*, 4158–4159.
- (90) OMEGA C++ Toolkit, 2.3.2; OpenEye Scientific Software, Inc.: Santa Fe, NM, 2008.
- (91) Thomas, A. H. Merck molecular force field. I. Basis, form, scope, parameterization, and performance of MMFF94. *J. Comput. Chem.* **1996**, *17*, 490–519.
- (92) Thomas, A. H. Merck molecular force field. II. MMFF94 van der Waals and electrostatic parameters for intermolecular interactions. *J. Comput. Chem.* **1996**, *17*, 520–552.
- (93) Thomas, A. H. Merck molecular force field. III. Molecular geometries and vibrational frequencies for MMFF94. *J. Comput. Chem.* **1996**, *17*, 553–586.

- (94) Thomas, A. H.; Robert, B. N. Merck molecular force field. IV. conformational energies and geometries for MMFF94. *J. Comput. Chem.* **1996**, *17*, 587–615.
- (95) Thomas, A. H. Merck molecular force field. V. Extension of MMFF94 using experimental data, additional computational data, and empirical rules. *J. Comput. Chem.* **1996**, *17*, 616–641.
- (96) Ferro, D. R.; Provasoli, A.; Ragazzi, M.; Casu, B.; Torri, G.; Bossenec, V.; Perly, B.; Sinay, P.; Petitou, M.; Choay, J. Conformer populations of L-iduronic acid residues in glycosaminoglycan sequences. *Carbohydr. Res.* **1990**, *195*, 157–167.
- (97) FRED (*Fast Rigid Exhaustive Docking*), 2.2.4; Openeye Scientific Software: Santa Fe, NM, 2008.
- (98) Esther, K.; Jordi, R.; Pascal, M.; Didier, R. Comparative evaluation of eight docking tools for docking and virtual screening accuracy. *Proteins* **2004**, *57*, 225–242.
- (99) Esko, J. D.; Linhardt, R. J. Proteins that bind sulfated glycosaminoglycans. In *Essentials of glycobiology*, II ed.; Varki, A., Cummings, R. D., Esko, J. D., Freeze, H. H., Stanley, P., Bertozzi, C. R., Hart, G. W., Etzler, M. E., Eds.; CSHL Press: New York, 2009.
- (100) Eldridge, M. D.; Murray, C. W.; Auton, T. R.; Paolini, G. V.; Mee, R. P. Empirical scoring functions: I. The development of a fast empirical scoring function to estimate the binding affinity of ligands in receptor complexes. *J. Comput. Aided Mol. Des.* **1997**, *11*, 425–445.
- (101) Gehlhaar, D. K.; Verkhivker, G. M.; Rejto, P. A.; Sherman, C. J.; Fogel, D. R.; Fogel, L. J.; Freer, S. T. Molecular recognition of the inhibitor AG-1343 by HIV-1 protease: conformationally flexible docking by evolutionary programming. *Chem. Biol.* **1995**, *2*, 317–324.
- (102) Stahl, M.; Rarey, M. Detailed analysis of scoring functions for virtual screening. *J. Med. Chem.* **2001**, *44*, 1035–1042.
- (103) Mark, R. M.; Harold, R. A.; Anthony, N.; Grant, J. A.; Frank, K. B. Gaussian docking functions. *Biopolymers* **2003**, *68*, 76–90.
- (104) Garrett, M. M.; David, S. G.; Robert, S. H.; Ruth, H.; William, E. H.; Richard, K. B.; Arthur, J. O. Automated docking using a Lamarckian genetic algorithm and an empirical binding free energy function. *J. Comput. Chem.* **1998**, *19*, 1639–1662.
- (105) Huey, R.; Morris, G. M.; Olson, A. J.; Goodsell, D. S. A semiempirical free energy force field with charge-based desolvation. *J. Comput. Chem.* **2007**, *28*, 1145–1152.
- (106) Alonso, H.; Bliznyuk, A. A.; Gready, J. E. Combining docking and molecular dynamic simulations in drug design. *Med. Res. Rev.* **2006**, *26*, 531–568.
- (107) Viktor, H.; Robert, A.; Asim, O.; Bentley, S.; Adrian, R.; Carlos, S. Comparison of multiple Amber force fields and development of improved protein backbone parameters. *Proteins* **2006**, *65*, 712–725.
- (108) Case, D. A.; Cheatham III, T. E.; Darden, T.; Gohlke, H.; Luo, R.; Merz, K. M., Jr.; Onufriev, A.; Simmerling, C.; Wang, B.; Woods, R. J. The Amber biomolecular simulation programs. *J. Comput. Chem.* **2005**, *26*, 1668–1688.
- (109) Wang, J.; Wolf, R.; Caldwell, J.; Kollman, P.; Case, D. Development and testing of a general amber force field. *J. Comput. Chem.* **2004**, *25*, 1157–74.
- (110) Kirschner, K. N.; Yongye, A. B.; Tschampel, S. M.; González-Outeiriño, J.; Daniels, C. R.; Foley, B. L.; Woods, R. J. GLYCAM06: A generalizable biomolecular force field. *Carbohydrates. J. Comput. Chem.* **2008**, *29*, 622–655.
- (111) Bayly, C. I.; Cieplak, P.; Cornell, W. D.; Kollman, P. A. A well-behaved electrostatic potential based method using charge restraints for deriving atomic charges: The RESP model. *J. Phys. Chem.* **1993**, *97*, 10269–10280.
- (112) Pigache, A.; Cieplak, P.; Dupradeau, F. Y., Automatic and highly reproducible RESP and ESP charge derivation: application to the development of programs RED and X RED. In *227th ACS National Meeting*, Anaheim, CA, March 28–April 1, 2004.
- (113) Frisch, M. J.; Trucks, G. W.; Schlegel, H. B.; Scuseria, G. E.; Robb, M. A.; Cheeseman, J. R.; Montgomery, J. A.; Vreven, J. T.; Kudin, K. N.; Burant, J. C.; Millam, J. M.; Iyengar, S. S.; Tomasi, J.; Barone, V.; Mennucci, B.; Cossi, M.; Scalmani, G.; Rega, N.; Petersson, G. A.; Nakatsuji, H.; Hada, M.; Ehara, M.; Toyota, K.; Fukuda, R.; Hasegawa, J.; Ishida, M.; Nakajima, T.; Honda, Y.; Kitao, O.; Nakai, H.; Klene, M.; Li, X.; Knox, J. E.; Hratchian, H. P.; Cross, J. B.; Bakken, V.; Adamo, C.; Jaramillo, J.; Gomperts, R.; Stratmann, R. E.; Yazyev, O.; Austin, A. J.; Cammi, R.; Pomelli, C.; Ochterski, J. W.; Ayala, P. Y.; Morokuma, K.; Voth, G. A.; Salvador, P.; Dannenberg, J. J.; Zakrzewski, V. G.; Dapprich, S.; Daniels, A. D.; Strain, M. C.; Farkas, O.; Malick, D. K.; Rabuck, A. D.; Raghavachari, K.; Foresman, J. B.; Ortiz, J. V.; Cui, Q.; Baboul, A. G.; Clifford, S.; Ciosowski, J.; Stefanov, B. B.; Liu, G.; Liashenko, A.; Piskorz, P.; Komaromi, I.; Martin, R. L.; Fox, D. J.; Keith, T.; Al-Laham, M. A.; Peng, C. Y.; Nanayakkara, A.; Challacombe, M.; Gill, P. M. W.; Johnson, B.; Chen, W.; Wong, M. W.; Gonzalez, C.; Pople, J. A. *Gaussian 03*, Revision C. 02; Gaussian, Inc.: Wallingford, CT, 2004.
- (114) Jorgensen, W. L.; Chandrasekhar, J.; Madura, J. D.; Impey, R. W.; Klein, M. L. Comparison of simple potential functions for simulating liquid water. *J. Chem. Phys.* **1983**, *79*, 926–935.
- (115) Nesmelova, I. V.; Sham, Y.; Gao, J.; Mayo, K. H. CXC and CC chemokines form mixed heterodimers: Association free energies from molecular dynamics simulations and experimental corelations. *J. Biol. Chem.* **2008**, *283*, 24155–24166.
- (116) Tsui, V.; Case, D. A. Theory and applications of the generalized Born solvation model in macromolecular simulations. *Biopolymers* **2001**, *56*, 257–291.
- (117) Sitkoff, D.; Sharp, K. A.; Honig, B. Accurate calculation of hydration free energies using macroscopic solvent models. *J. Phys. Chem.* **1994**, *98*, 1978–1988.
- (118) Sanner, M. F.; Olson, A. J.; Spehner, J.-C. Reduced surface: An efficient way to compute molecular surfaces. *Biopolymers* **1996**, *38*, 305–320.
- (119) Nguyen, D. T.; Case, D. A. On finding stationary states on large-molecule potential energy surfaces. *J. Phys. Chem.* **1985**, *89*, 4020–4026.
- (120) Eric, F. P.; Thomas, D. G.; Conrad, C. H.; Gregory, S. C.; Daniel, M. G.; Elaine, C. M.; Thomas, E. F. UCSF Chimera - A visualization system for exploratory research and analysis. *J. Comput. Chem.* **2004**, *25*, 1605–1612.
- (121) Chen, M. E.; Cang, H. X.; Nymeyer, H. NOC, 3.0.; Institute of Molecular Biology, Florida State University: FL, 2007.
- (122) Kanagarajadurai, K.; Sowdhamini, R. Sequence and structural analyses of interleukin-8-like chemokine superfamily. *In Silico Biol.* **2008**, *8*, 307–330.
- (123) Kagtiampakis, I.; Jin, H.; Kim, S.; Vannucci, M.; LiWang, P. J.; Tsai, J. Conservation of unfavorable sequence motifs that contribute to the chemokine quaternary state. *Biochemistry* **2008**, *47*, 10637–10648.
- (124) Laguri, C.; Arenzana-Seisdedos, F.; Lortat-Jacob, H. Relationships between glycosaminoglycan and receptor binding sites in chemokines—the CXCL12 example. *Carbohydr. Res.* **2008**, *343*, 2018–2023.
- (125) Brändén, C.-I.; Tooze, J. *Introduction to protein structure*, II ed.; Garland Pub.: New York, 1999; p 410.
- (126) Goldenberg, O.; Erez, E.; Nimrod, G.; Ben-Tal, N. The ConSurf-DB: pre-calculated evolutionary conservation profiles of protein structures. *Nucleic Acids Res.* **2009**, *37*, D323–D327.
- (127) Inoue, Y.; Endo, M.; Haruta, C.; Taniuchi, T.; Moritomo, T.; Nakanishi, T. Molecular cloning and sequencing of the silver chimaera (Chimaera phantasma) interleukin-8 cDNA. *Fish Shellfish Immunol.* **2003**, *15*, 269–274.
- (128) Lee, E.-Y.; Park, H.-H.; Kim, Y.-T.; Chung, J.-K.; Choi, T.-J. Cloning and sequence analysis of the interleukin-8 gene from flounder (Paralichthys olivaceus). *Gene* **2001**, *274*, 237–243.
- (129) Covello, J. M.; Bird, S.; Morrison, R. N.; Battaglene, S. C.; Secombe, C. J.; Nowak, B. F. Cloning and expression analysis of three striped trumpeter (*Latris lineata*) pro-inflammatory cytokines, TNF- α , IL-1 β and IL-8, in response to infection by the ectoparasitic, *Chondracanthus goldsmithi*. *Fish Shellfish Immunol.* **2009**, *26*, 773–786.
- (130) Sepulcre, M. P.; Sarropoulou, E.; Kotoulas, G.; Meseguer, J.; Mulero, V. *Vibrio anguillarum* evades the immune response of the bony fish sea bass (*Dicentrarchus labrax* L.) through the inhibition of leukocyte respiratory burst and down-regulation of apoptotic caspases. *Mol. Immunol.* **2007**, *44*, 3751–3757.

- (131) Wu, Y. F.; Shien, J. H.; Yin, H. H.; Chiow, S. H.; Lee, L. H. Structural and functional homology among chicken, duck, goose, turkey and pigeon interleukin-8 proteins. *Vet. Immunol. Immunopathol.* **2008**, *125*, 205–215.
- (132) Liu, Y.; Yang, S.; Lin, A.; Cavalli-Sforza, L.; Su, B. Molecular evolution of CXCR1, a G protein-coupled receptor involved in signal transduction of neutrophils. *J. Mol. Evol.* **2005**, *61*, 691–696.
- (133) Shields, D. C. Gene conversion among chemokine receptors. *Gene* **2000**, *246*, 239–245.
- (134) Zlotnik, A.; Yoshie, O.; Nomiyama, H. The chemokine and chemokine receptor superfamilies and their molecular evolution. *Genome Biol.* **2006**, *7*, 243.
- (135) DeVries, M. E.; Kelvin, A. A.; Xu, L.; Ran, L.; Robinson, J.; Kelvin, D. J. Defining the origins and evolution of the Chemokine/Chemokine receptor system. *J. Immunol.* **2006**, *176*, 401–415.
- (136) Suzuki, H.; Prado, G. N.; Wilkinson, N.; Navarro, J. The N terminus of interleukin-8 (IL-8) receptor confers high affinity binding to human IL-8. *J. Biol. Chem.* **1994**, *269*, 18263–18266.
- (137) Reeves, E. P.; Williamson, M.; Byrne, B.; Bergin, D. A.; Smith, S. G. J.; Greally, P.; O'Kennedy, R.; O'Neill, S. J.; McElvaney, N. G. IL-8 dictates glycosaminoglycan binding and stability of IL-18 in cystic fibrosis. *J. Immunol.* **2010**, *184*, 1642–1652.
- (138) Caldwell, E. E. O.; Nadkarni, V. D.; Fromm, J. R.; Linhardt, R. J.; Weiler, J. M. Importance of specific amino acids in protein binding sites for heparin and heparan sulfate. *Int. J. Biochem. Cell Biol.* **1996**, *28*, 203–216.
- (139) Fromm, J. R.; Hileman, R. E.; Caldwell, E. E. O.; Weiler, J. M.; Linhardt, R. J. Pattern and spacing of basic amino acids in heparin binding sites. *Arch. Biochem. Biophys.* **1997**, *343*, 92–100.
- (140) Cardin, A. D.; Weintraub, H. J. Molecular modeling of protein-glycosaminoglycan interactions. *Arterioscler. Thromb. Vasc. Biol.* **1989**, *9*, 21–32.
- (141) Ronald, E. H.; Jonathan, R. F.; John, M. W.; Robert, J. L. Glycosaminoglycan-protein interactions: definition of consensus sites in glycosaminoglycan binding proteins. *BioEssays* **1998**, *20*, 156–167.
- (142) Margalit, H.; Fischer, N.; Ben-Sasson, S. A. Comparative analysis of structurally defined heparin binding sequences reveals a distinct spatial distribution of basic residues. *J. Biol. Chem.* **1993**, *268*, 19228–19231.
- (143) Forster, M.; Mulloy, B. Computational approaches to the identification of heparin-binding sites on the surfaces of proteins. *Biochem. Soc. Trans.* **2006**, *34*, 431–434.
- (144) Williams, G.; Borkakoti, N.; Bottomley, G. A.; Cowan, I.; Fallowfield, A. G.; Jones, P. S.; Kirtland, S. J.; Price, G. J.; Price, L. Mutagenesis studies of interleukin-8. Identification of a second epitope involved in receptor binding. *J. Biol. Chem.* **1996**, *271*, 9579–9586.
- (145) Clark-Lewis, I.; Schumacher, C.; Baggolini, M.; Moser, B. Structure-activity relationships of interleukin-8 determined using chemically synthesized analogs. Critical role of NH₂-terminal residues and evidence for uncoupling of neutrophil chemotaxis, exocytosis, and receptor binding activities. *J. Biol. Chem.* **1991**, *266*, 23128–23134.
- (146) Schug, A.; Herges, T.; Wenzel, W. Reproducible protein folding with the stochastic tunneling method. *Phys. Rev. Lett.* **2003**, *91*, 158102.
- (147) Herges, T.; Wenzel, W. An all-atom force field for tertiary structure prediction of helical proteins. *Biophys. J.* **2004**, *87*, 3100–3109.
- (148) Meliciani, I.; Klenin, K.; Strunk, T.; Schmitz, K.; Wenzel, W. Probing hot spots on protein-protein interfaces with all-atom free-energy simulation. *J. Chem. Phys.* **2009**, *131*, 034114.
- (149) Swanson, J. M.; Henchman, R. H.; McCammon, J. A. Revisiting free energy calculations: a theoretical connection to MM/PBSA and direct calculation of the association free energy. *Biophys. J.* **2004**, *86*, 67–74.
- (150) Benedix, A.; Becker, C. M.; de Groot, B. L.; Caflisch, A.; Bockmann, R. A. Predicting free energy changes using structural ensembles. *Nat. Methods* **2009**, *6*, 3–4.
- (151) Yap, K. L.; Ames, J. B.; Swindells, M. B.; Ikura, M. Vector geometry mapping. A method to characterize the conformation of helix-loop-helix calcium-binding proteins. *Methods Mol. Biol.* **2002**, *173*, 317–324.
- (152) Clore, G. M.; Gronenborn, A. M. Comparison of the solution nuclear magnetic resonance and crystal structures of interleukin-8. Possible implications for the mechanism of receptor binding. *J. Mol. Biol.* **1991**, *217*, 611–620.
- (153) Rajarathnam, K.; Clark-Lewis, I.; Dewald, B.; Baggolini, M.; Sykes, B. D. ¹H NMR evidence that Glu-38 interacts with the N-terminal functional domain in interleukin-8. *FEBS Lett.* **1996**, *399*, 43–46.
- (154) Rajarathnam, K.; Clark-Lewis, I.; Sykes, B. D. ¹H NMR studies of interleukin 8 analogs: characterization of the domains essential for function. *Biochemistry* **1994**, *33*, 6623–6630.
- (155) Cornell, W. D.; Cieplak, P.; Bayly, C. I.; Gould, I. R.; Merz, K. M.; Ferguson, D. M.; Spellmeyer, D. C.; Fox, T.; Caldwell, J. W.; Kollman, P. A. A second generation force field for the simulation of proteins, nucleic acids, and organic molecules. *J. Am. Chem. Soc.* **1995**, *117*, 5179–5197.
- (156) Wang, J.; Cieplak, P.; Kollman, P. A. How well does a restrained electrostatic potential (RESP) model perform in calculating conformational energies of organic and biological molecules? *J. Comput. Chem.* **2000**, *21*, 1049–1074.
- (157) García, A. E.; Sanbonmatsu, K. Y. α -Helical stabilization by side chain shielding of backbone hydrogen bonds. *Proc. Natl. Acad. Sci. U.S.A.* **2002**, *99*, 2782–2787.
- (158) Ono, S.; Nakajima, N.; Higo, J.; Nakamura, H. Peptide free-energy profile is strongly dependent on the force field: Comparison of C96 and AMBER95. *J. Comput. Chem.* **2000**, *21*, 748–762.
- (159) Lindorff-Larsen, K.; Piana, S.; Palmo, K.; Maragakis, P.; Klepeis, J. L.; Dror, R. O.; Shaw, D. E. Improved side-chain torsion potentials for the Amber ff99SB protein force field. *Proteins* **2010**, *78*, 1950–1958.
- (160) Wickstrom, L.; Okur, A.; Simmerling, C. Evaluating the performance of the ff99SB force field based on NMR scalar coupling data. *Biophys. J.* **2009**, *97*, 853–856.
- (161) Best, R. B.; Buchete, N.-V.; Hummer, G. Are current molecular dynamics force fields too helical?. *Biophys. J.* **2008**, *95* L07–L09.
- (162) Showalter, S. A.; Johnson, E.; Rance, M.; Brüschweiler, R. Toward quantitative interpretation of methyl side-chain dynamics from NMR by molecular dynamics simulations. *J. Am. Chem. Soc.* **2007**, *129*, 14146–14147.
- (163) Wickstrom, L.; Okur, A.; Song, K.; Hornak, V.; Raleigh, D. P.; Simmerling, C. L. The unfolded state of the villin headpiece helical subdomain: Computational studies of the role of locally stabilized structure. *J. Mol. Biol.* **2006**, *360*, 1094–1107.
- (164) Wolfgang, K.; Christian, S. Dictionary of protein secondary structure: Pattern recognition of hydrogen-bonded and geometrical features. *Biopolymers* **1983**, *22*, 2577–2637.
- (165) Grasberger, B. L.; Gronenborn, A. M.; Clore, G. M. Analysis of the backbone dynamics of interleukin-8 by ¹⁵N relaxation measurements. *J. Mol. Biol.* **1993**, *230*, 364–372.
- (166) Woods, R. J.; Tessier, M. B. Computational glycoscience: characterizing the spatial and temporal properties of glycans and glycan-protein complexes. *Curr. Opin. Struct. Biol.* **2010**, *20*, 575–83.
- (167) Gandhi, N. S.; Mancera, R. L. Free energy calculations of glycosaminoglycan-protein interactions. *Glycobiology* **2009**, *19*, 1103–1115.
- (168) Kerzmann, A.; Fuhrmann, J.; Kohlbacher, O.; Neumann, D. BALLDock/SLICK: a new method for protein-carbohydrate docking. *J. Chem. Inf. Model.* **2008**, *48*, 1616–1625.
- (169) Kerzmann, A.; Neumann, D.; Kohlbacher, O. SLICK--scoring and energy functions for protein-carbohydrate interactions. *J. Chem. Inf. Model.* **2006**, *46*, 1635–1642.
- (170) Laederach, A.; Reilly, P. J. Specific empirical free energy function for automated docking of carbohydrates to proteins. *J. Comput. Chem.* **2003**, *24*, 1748–1757.
- (171) Rao, V. S. R.; Qasba, P. K.; Balaji, P. V.; Chandrasekaran, R. *Conformation of carbohydrates*; Harwood Academic Pub: Amsterdam, 1998; p 409.
- (172) Fadda, E.; Woods, R. J. Molecular simulations of carbohydrates and protein-carbohydrate interactions: motivation, issues and prospects. *Drug Discov. Today* **2010**, *15*, 596–609.

- (173) Day, R.; Paschek, D.; Garcia, A. E. Microsecond simulations of the folding/unfolding thermodynamics of the Trp-cage miniprotein. *Proteins* **2010**, *78*, 1889–1899.
- (174) Hess, B.; van der Vegt, N. F. Hydration thermodynamic properties of amino acid analogues: a systematic comparison of biomolecular force fields and water models. *J. Phys. Chem. B* **2006**, *110*, 17616–17626.
- (175) Murphy, J. W.; Cho, Y.; Sachpatzidis, A.; Fan, C.; Hodsdon, M. E.; Lolis, E. Structural and Functional Basis of CXCL12 (Stromal Cell-derived Factor-1 α) Binding to Heparin. *J. Biol. Chem.* **2007**, *282*, 10018–10027.
- (176) Ohnishi, Y.; Senda, T.; Nandhagopal, N.; Sugimoto, K.; Shioda, T.; Nagai, Y.; Mitsui, Y. Crystal Structure of Recombinant Native SDF-1 α with Additional Mutagenesis Studies: An Attempt at a More Comprehensive Interpretation of Accumulated Structure-Activity Relationship Data. *J. Interferon Cytokine Res.* **2000**, *20*, 691–700.
- (177) Malik, Z. A.; Tack, B. F. Structure of human MIP-3 α chemokine. *Acta Cryst. Sect. F* **2006**, *62*, 631–634.
- (178) Barinka, C.; Prahl, A.; Lubkowski, J. Structure of human monocyte chemoattractant protein 4 (MCP-4/CCL13). *Acta Cryst. Sect. D* **2008**, *64*, 273–278.
- (179) Wilken, J.; Hoover, D.; Thompson, D. A.; Barlow, P. N.; McSparron, H.; Picard, L.; Wlodawer, A.; Lubkowski, J.; Kent, S. B. H. Total chemical synthesis and high-resolution crystal structure of the potent anti-HIV protein AOP-RANTES. *Chem. Biol.* **1999**, *6*, 43–51.
- (180) Shaw, J. P.; Johnson, Z.; Borlat, F.; Zwahlen, C.; Kungl, A.; Roulin, K.; Harrenga, A.; Wells, T. N. C.; Proudfoot, A. E. I. The X-Ray Structure of RANTES: Heparin-Derived Disaccharides Allows the Rational Design of Chemokine Inhibitors. *Structure* **2004**, *12*, 2081–2093.